جامعة الجوف
Jouf University

# Jouf University Science and Engineering Journal

# (JUSEJ)

## Peer-Reviewed International Journal
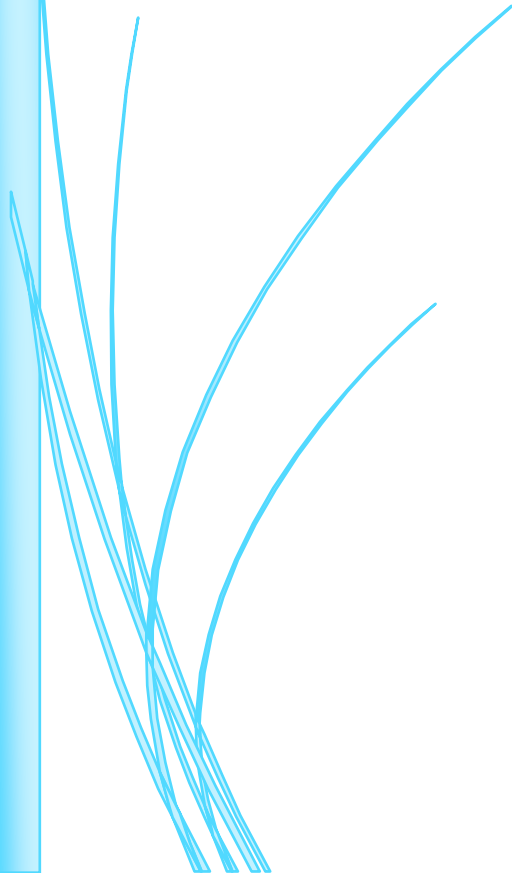
# Jouf University Science and Engineering Journal

*Peer-reviewed International Journal*

*Designed and Edited by Prof. Abdelazim M. Mebed*

من سورة يوسف - الآية: 76

*Dear professional colleagues, researchers and fellow students:*

We are pleased to present the second issue of Volume VIII of the Journal of Science and Engineering (JUSEJ). JUSEJ was established under the generous sponsorship of the former rector of Jouf University, Prof. Ismail Muhammad Al-Bishri, since 2014, and the continuous support of the current president of the University, Prof. Muhammad Al-Shaya. Its maturity is an outcome of the consistent support of high-performing authors, a supportive and professional dedicated reviewers, many vigorous and conscientious editorial boards and collective input from the editorial board members. Various researchers who are active in the above field have been enrolled for providing the necessary impetus for the new journal. We are quite hopeful and shall be grateful to the service that these eminent scientists shall provide to the growth of JUSEJ. We are certain that the renowned scientists and academicians both from the industry and academic institutions all over the world will be enriched by sharing their research experiences through JUSEJ. We are happy to invite you to submit your valuable research works in URP journals. We strongly believe that our journal will help to develop your own professional career.

*Thanks*
*Editors*

## Editorial Board

## Focus and Scope

With its vision to promote science and scientific knowledge to everybody, Jouf Science and Engineering Journal (JUSEJ) is an international peer-reviewed journal owned by Jouf University with a focused aim of promoting and publishing original high quality research papers dealing with basic and engineering science. JUSEJ publishes rigorous and original contributions in the Science disciplines of

| | | |
|---|---|---|
| Physics | Engineering, All Fields | Applied Biology |
| Chemistry | Mathematics & Statistics | Physiology |
| Biochemistry | Computer Science | Plant Biology |
| Biological Sciences | Genomics | Population Biology |
| Biophysics | Geology | Food & Food Technology |
| Petroleum & Gas | Environment | Robotics |
| Cell Biology | Solid State Technology | Signal Transduction |
| Parasitological Science | Communication & IT | Space Science |
| Developmental Biology | Microbiology | Energy |
| Genetics | Zoology | Textile Industry & Fabrics |
| Construction | Nanotechnology | Toxicology |

The papers published in Jouf Science and Engineering Journal (JUSEJ) should present novel results and have either theoretical significance or practical utility or both. They may be presented in the form of full articles, short communications or state-of-the-art reviews.

 All contributions will be rigorously reviewed to ensure both scientific quality and technical relevance. Revisions of manuscripts may thus be required.

Manuscripts must be submitted in the English language and authors must ensure that the article has not been published or submitted for publication elsewhere in any format, and that there are no ethical concerns with the contents or data collection. The authors warrant that the information submitted is not redundant and respects general guidelines of ethics in publishing. All papers are evaluated by at least two international referees, who are known scholars in their fields.

## Objectives

The main objective of JUSEJ is to provide an international forum for academics, researchers, industry leaders, and policy makers to investigate and exchange novel ideas and disseminate knowledge and information covering the broad range of natural science and industrial activities. In addition, it aims to establish an effective channel of communication between policy makers, government agencies, academic and research institutions and persons concerned with basic science and its applications. It also aims to promote and coordinate developments in the fields of natural science, engineering science and other related fields. The international dimension is emphasized in order to overcome cultural and national barriers and to meet the needs of accelerating ecological and technological advances in all industries and the global society and economy.

## Open Access Policy

This journal provides immediate open access to its content on the principle that making research freely available to the public supports a greater global exchange of knowledge.

All published manuscripts will be available on the Journals website **http://vrgs.ju.edu.sa/#**. We strongly believe that our journal will help to develop your own professional career. You can communicate with us at any time, throughout the publishing process.

## EDITORIAL OFFICE & COMMUNICATION

**Jouf Science and Engineering Journal (JUSEJ)**

 Jouf University, Sakaka, 2014, Aljouf, Saudi Arabia

**Email:** ajbse@*ju.edu.sa*

# TABLE OF CONTENTS

# GUIDE FOR AUTHOR

## TYPES OF CONTRIBUTIONS

Original research papers and occasional reviews, short communications, letters, letters to the editor and news items. Please ensure that you indicate clearly the appropriate article type when making your submission.

## BEFORE YOU BEGIN

### *Ethical guidelines*
### Confidentiality
All material submitted to Science Journal of Jouf University (SJJU), accordingly to Jouf Science, Engineering Journal (JUSEJ) remains confidential, and the Editor operates a peer review system in which the identity of the referees is protected.

### Duplicate publication
Duplicate publication is the publication of the same paper or substantially similar papers in more than one journal. Authors must explain in the submission letter any prior publication of the same or a substantially similar paper, and should explain any circumstances that might lead the Editor or reviewers to believe that the paper may have been published elsewhere (for example, when the title of a submitted paper is the same as or similar to the title of a previously published article).

If work that makes up more than 10% of the manuscript submitted to JUSEJ has been published elsewhere, please provide a copy of the published article in order that the Editor can make a judgment on the amount of overlap without delay. If a member of the editorial board learns that work under consideration has previously been published in whole or in part,

the Editor may return the paper without review, reject the paper, announce the duplication publicly in an editorial and/or contact the authors' employers.

### Submission of manuscripts to more than one journal
Authors may not send the same manuscript to more than one journal concurrently. If this occurs, the Editor may return the paper without review, reject the paper, contact the Editor of the other journal(s) in question and/or contact the authors' employers.

### Plagiarism and scientific misconduct
Plagiarism is the use of others' published and unpublished ideas or words (or other intellectual property) without due reference or permission and/or their presentation as new and original points. Plagiarism is serious scientific misconduct and will be dealt with accordingly. All papers submitted to the journal is cheched with *iThenticate* program for plagiarism. We define plagiarism as a case in which a paper reproduces another work with at least 15% similarity and without citation.

If evidence of plagiarism is found before or after acceptance or after publication of the paper, the author will be offered a chance to defend his/her paper. If the arguments are found to be unsatisfactory, the manuscript will be retracted and authors found to have been guilty of plagiarism will no longer have papers accepted for publication by JUSEJ.



iThenticate compares submitted documents to extensive data repositories to create a

comprehensive Similarity Report, which highlights and provides links to any significant text matches, helping to ensure that you are submitting an original and well-attributed document.

### Data auditing

The journal reserves the right to view original figures and data and may make periodic requests to see these.

### Conflict of interest

All authors are requested to disclose any actual or potential conflict of interest including any financial, personal or other relationships with other people or organizations within three years of beginning the submitted work that could inappropriately influence, or be perceived to influence, their work.

### Submission declaration

Submission of an article implies that the work described has not been published previously (except in the form of an abstract or as part of a published lecture or academic thesis or as an electronic preprint, that it is not under consideration for publication elsewhere, that its publication is approved by all authors and tacitly or explicitly by the responsible authorities where the work was carried out, and that, if accepted, it will not be published elsewhere including electronically in the same form, in English or in any other language, without the written consent of the copyright-holder.

### Changes in authorship

Requests to add or remove an author, or to rearrange the author names, must be sent to the Journal Manager from the corresponding author of the accepted manuscript *before the accepted manuscript is published* and must include: (a) the reason for the addition, removal, or rearrangement of the authors' names and (b) written confirmation (e-mail, fax, letter) from all authors that they agree with the addition,

removal or rearrangement. In the case of addition or removal of authors, this includes confirmation from the author being added or removed. Requests that are not sent by the corresponding author will be forwarded by the Journal Manager to the corresponding author, who must follow the procedure as described above. Note that: (1) Journal Managers will inform the Journal Editors of any such requests and (2) publication of the accepted manuscript is suspended until authorship has been agreed.

### Copyright

Upon acceptance of an article, authors will be asked to complete a 'Journal Publishing Agreement' An e-mail will be sent to the corresponding author confirming receipt of the manuscript together with a 'Journal Publishing Agreement'.

Subscribers may reproduce tables of contents or prepare lists of articles, including abstracts for internal circulation within their institutions. Permission of the Publisher is required for resale or distribution outside the institution and for all other derivative works, including compilations and translations.

If excerpts from other copyrighted works are included, the author(s) must obtain written permission from the copyright owners and credit the source(s) in the article.

### Retained author rights

As an author you (or your employer or institution) have the right to use your articles for a wide range of scholarly purposes.

### Role of the funding source

You are requested to identify who provided financial support for the conduct of the research and/or preparation of the article and to briefly describe the role of the sponsor(s), if any, in study design; in the collection, analysis and interpretation of data; in the writing of the report; and in the decision to submit the article

for publication. If the funding source(s) had no such involvement then this should be stated

**Subscription**
Articles are made available to subscribers as well as developing countries and patient groups

*Language (usage and editing services)*
Please write your text in good English (American or British usage is accepted, but not a mixture of these). If the English language is used, extra abstract in Arabic should be provided.

*Submission*
To submit your paper, please send your manuscripts by e-mail to the Editor (AJBSE@ju.edu.sa). You must submit the manuscript in a single electronic file. The manuscript should be edited using Microsoft (MS) Word (2003 up to 2010, with .doc or .docx extension)

*Referees*
Please submit, with the manuscript, the names, addresses and e-mail addresses of three potential referees. Note that the Editor retains the only one who has the right to decide whether or not the suggested reviewers are used.

## PREPARATION

*Use of word processing software*
Manuscripts must be in an electronic format that meets the following specifications:

- Do not submit a manuscript file as a PDF file. Remove line numbering.
- The manuscript file—with tables and figures placed at the end of the file, each on a separate page—should be in Microsoft Word (2003 up to 2010, with .doc or .docx extension).
- Do not use the Microsoft Word "Styles and Formatting" or "Track Changes" features in the file.

- Tables should be in MS Word (.doc or .docx), one table to a page using hard page breaks.
- Figures (graphics of any kind) should be placed at the end of the Word document as images, one figure to a page using hard page breaks.
- Equations may be created and inserted as part of the text, or they may be submitted as images embedded within the text.

## ARTICLE STRUCTURE

**Manuscript Page setup**
- Margins: 25.4 mm (1 in.) top, 25.4 mm (1 in.) left; adjust the settings for bottom and right margins so that the text area is not more than 165.1 mm by 228.6 mm (6.5 in. by 9 in.)
- Font (typeface): Times New Roman, no smaller than 10 points.
- Numbering: Insert page numbers at upper right of each page; insert name(s) of author(s) at upper left of each page
- Text: Single-spaced.
- Paragraphs: Indent first line 12.7 mm (0.5 in.); do not use an extra line space between paragraphs; do not indent first line after a subhead.

Subheads: All subheads should be flush with the left margin, with one line space above. Subsections should be numbered 1.1 (then 1.1.1, 1.1.2, ...), 1.2, etc. (the abstract is not included in section numbering).

**FIRST-LEVEL SUBHEAD**
(all capitals, boldface, on separate line)
**Second-Level Subhead**
(initial capitals, boldface, on separate line)
*Third-Level Subhead*
(initial capitals, italic, on separate line)

**Fourth-Level Subhead** (initial capitals, boldface, on same line as text, with extra letter space between the subhead and text)

*Fifth-Level Subhead* (initial capitals, italic, on same line as text, with extra letter space between the subhead and text)

• Bulleted and numbered lists: Indent first line 12.7 mm (0.5 in.); do not indent for text runovers.

**Table Titles and Figure Captions:**

**TABLE 5 Effects of All Factors**
(Insert title above the table; "Table" is all capitals; title is initial capitals; all types are boldfaced;

Extra space, but no punctuation after number; no punctuation at end of title.)

**FIGURE 3 Example of results**.
(Insert caption below the figure; "Figure" is all capitals; caption is sentence case; all type is boldface; extra space but no punctuation after number; period at end of caption.)

**Body of the manuscript**

*Introduction*
State the objectives of the work and provide an adequate background, avoiding a detailed literature survey or a summary of the results.

*Materials and methods*
Provide sufficient detail to allow the work to be reproduced. Methods already published should be indicated by a reference: only relevant modifications should be described.

*Theory/calculation*
A Theory section should extend, not repeat, the background to the article already dealt with in the Introduction and lay the foundation for further work. In contrast, a Calculation section represents a practical development from a theoretical basis.

*Results*
Results should be clear and concise.

*Discussion*
This should explore the significance of the results of the work, not repeat them. A combined Results and Discussion section is often appropriate. Avoid extensive citations and discussion of published literature.

*Conclusions*
The main conclusions of the study may be presented in a short Conclusions section, which may stand alone or form a subsection of a Discussion or Results and Discussion section.

*Appendices*
If there is more than one appendix, they should be identified as A, B, etc. Formulae and equations in appendices should be given separate numbering: Eq. (A.1), Eq. (A.2), etc.; in a subsequent appendix, Eq. (B.1) and so on. Similarly for tables and figures: Table A.1; Fig. A.1, etc.

***Essential title page information***
• ***Title.*** Concise and informative. Titles are often used in information-retrieval systems. Avoid
abbreviations and formulae where possible. The title should be all capitals.
• ***Author names and affiliations.*** Where the family name may be ambiguous (e.g., a double name), please indicate this clearly. Present the authors' affiliation addresses (where the actual work was done) below the names. Indicate all affiliations with a lower-case superscript letter immediately after the author's name and in front of the appropriate address. Provide the full postal address of each affiliation, including the

country name, and, if available, the e-mail address of each author.

• *Corresponding author.* Clearly indicate who will handle correspondence at all stages of refereeing and publication, also post-publication. **Ensure that phone numbers (with country and area code) are provided in addition to the e-mail address and the complete postal address. Contact details must be kept up to date by the corresponding author.**

• *Present/permanent address.* If an author has moved since the work described in the article was done, or was visiting at the time, a 'Present address' (or 'Permanent address') may be indicated as a footnote to that author's name. The address at which the author actually did the work must be retained as the main, affiliation address. Superscript Arabic numerals are used for such footnotes.

### Abstract

A concise and factual abstract is required. The abstract should state briefly the purpose of the research, the principal results and major conclusions. An abstract is often presented separately from the article, so it must be able to stand alone. For this reason, References should be avoided, but if essential, then cite the author(s) and year(s). Also, non-standard or uncommon abbreviations should be avoided, but if essential they must be defined at their first mention in the abstract itself.

### Keywords

Immediately after the abstract, provide a maximum of 6 keywords, using American spelling and

avoiding general and plural terms and multiple concepts (avoid, for example, 'and', 'of'). Be sparing with abbreviations: only abbreviations firmly established in the field may be eligible. These keywords will be used for indexing purposes.

### Abbreviations

Define abbreviations that are not standard in this field in a footnote to be placed on the first page of the article. Such abbreviations that are unavoidable in the abstract must be defined at their first mention there, as well as in the footnote. Ensure consistency of abbreviations throughout the article.

### Acknowledgements

Collate acknowledgements in a separate section at the end of the article before the references and do not, therefore, include them on the title page, as a footnote to the title or otherwise. List here those individuals who provided help during the research (e.g., providing language help, writing assistance or proof reading the article, etc.).

### Nomenclature and units

Follow internationally accepted rules and conventions: use the international system of units (SI).
If other quantities are mentioned, give their equivalent in SI.

### Math formulae

Present simple formulae in the line of normal text where possible and use the solidus (/) instead of a horizontal line for small fractional terms, e.g., X/Y. In principle, variables are to be presented in italics. Powers of e are often more conveniently denoted by exp. Number consecutively any equations that have to be displayed separately from the text (if referred to explicitly in the text).

### Footnotes

Footnotes should be used sparingly. Number them consecutively throughout the article, using superscript Arabic numbers. Many word processors build footnotes into the text, and this feature may be used. Should this not be the case, indicate the position of footnotes in the text and present the footnotes themselves separately at

the end of the article. Do not include footnotes in the Reference list.

### Table footnotes

Indicate each footnote in a table with a superscript lowercase letter.

### Tables

Number tables consecutively in accordance with their appearance in the text. Place footnotes to tables below the table body and indicate them with superscript lowercase letters. Avoid vertical rules. Be sparing in the use of tables and ensure that the data presented in tables do not duplicate results described elsewhere in the article.

### References

*Citation in text*

Please ensure that every reference cited in the text is also present in the reference list (and *vice versa*). Any references cited in the abstract must be given in full. Unpublished results and personal communications are not recommended in the reference list, but may be mentioned in the text. If these references are included in the reference list they should follow the standard reference style of the journal and should include a substitution of the publication date with either 'Unpublished results' or 'Personal communication'. Citation of a reference as 'in press' implies that the item has been accepted for publication.

### Web references

As a minimum, the full URL should be given and the date when the reference was last accessed. Any further information, if known (DOI, author names, dates, reference to a source publication, etc.), should also be given. Web references can be listed separately (e.g., after the reference list) under a different heading if desired, or can be included in the reference list.

*References in a special issue*

Please ensure that the words 'this issue' are added to any references in the list (and any citations in the text) to other articles in the same Special Issue.

*Reference style*

*Text:* Indicate references by number(s) in square brackets in line with the text. The actual authors can be referred to, but the reference number(s) must always be given. Example: '..... as demonstrated [3,6]. Barnaby and Jones [8] obtained a different result ....'

*List:* Number the references (numbers in square brackets) in the list in the order in which they appear in the text.

*Examples:*

Reference to a journal publication:
[1] J. van der Geer, J.A.J. Hanraads, R.A. Lupton, The art of writing a scientific article, J. Sci. Commun. 163 (2010) 51–59.
Reference to a book:
[2] W. Strunk Jr., E.B. White, The Elements of Style, fourth ed., Longman, New York, 2000.
Reference to a chapter in an edited book:
[3] G.R. Mettam, L.B. Adams, How to prepare an electronic version of your article, In: B.S. Jones, R.Z. Smith (Eds.), Introduction to the Electronic Age, E-Publishing Inc., New York, 2009, pp. 281–304.

*Journal abbreviations source*

Journal names should be abbreviated according to the List of title word abbreviations http://www.sciencemag.org/site/feature/contribinfo/prep/res/journal_abbrevs.xhtml

### Submission checklist

The following list will be useful during the final checking of an article prior to sending it to the journal for review. Please consult this Guide for Authors for further details of any item.
**Ensure that the following items are present:**
One author has been designated as the corresponding author with contact details:
• E-mail address

• Full postal address
• Phone numbers
• Keywords
Further considerations
• Manuscript has been 'spell-checked' and 'grammar-checked'
• References are in the correct format for this journal
• All references mentioned in the Reference list are cited in the text, and *vice versa*
• Permission has been obtained for use of copyrighted material from other sources (including the Web)
• Color figures are clearly marked as being intended for color reproduction

## AFTER ACCEPTANCE

### Proofs

One set of page proofs (as PDF files) will be sent by e-mail to the corresponding author (if we do not have an e-mail address then paper proofs will be sent by post). If there is any correction, please list your corrections quoting line number. If, for any reason, this is not possible, then mark the corrections and any other comments on a printout of your proof and return by fax, or scan the pages and e-mail, or by post. Please use this proof only for checking the typesetting, editing, completeness and correctness of the text, tables and figures. Significant changes to the article as accepted for publication will only be considered at this stage with permission from the Editor. We will do everything possible to get your article published quickly and accurately – please let us have all your corrections within 48 hours. It is important to ensure that all corrections are sent back to us in one communication: please check carefully before replying, as inclusion of any subsequent corrections cannot be guaranteed. Proofreading is solely your responsibility.

### Offprint

The corresponding author, at no cost, will be provided with a PDF file of the article *via* email (the PDF file is a watermarked version of the published article and includes a cover sheet with the journal cover image and a disclaimer outlining the terms and conditions of use). For an extra charge, paper offprints can be ordered via the offprint order form which is sent once the article is accepted for publication. Both corresponding and co-authors may order offprints at any time *via* e-mail (ajbse@ju.edu.sa)

## AUTHOR INQUIRIES

For inquiries relating to the submission of articles (including electronic submission) please visit this journal's homepage. Contact details for questions arising after acceptance of an article, especially those relating to proofs, will be provided by the publisher.

## DISCLAIMER

**Jouf Science and Engineering Journal** shall not take any responsibility for the contents of articles published in the journal and all such responsibility shall lie with the author/s. The opinions expressed in the articles are solely of the author/s and **JUSEJ** may not agree with such opinions in part or in full.

# REDUCED-COMPLEXITY SELECTIVE MAPPING SCHEME FOR PEAK TO AVERAGE POWER RATIO REDUCTION IN FILTER BANK MULTI-CARRIER SYSTEMS

## Emad S. Hassan [1*]

[1]Department of Electrical Engineering, College of Engineering, Jazan University, Jizan 45142, Saudi Arabia;

### *Corresponding author

*Emad S. Hassan*

### Email address:

*eshassan@jazanu.edu.sa*

**Submission Date**:     *Mar. 22, 2022.*
**Accepted Date:**       *April. 12, 2022*

Filter Bank Multi-Carrier (FBMC) has attracted considerable attention for future communication systems. However, like any multicarrier modulation (MCM), it exhibits a high peak-to-average power ratio (PAPR). This paper proposes a novel reduced complexity selective mapping (RC-SLM) scheme for PAPR reduction in FBMC. The basic idea of the RC-SLM scheme is to divide the frequency domain data symbols into different sub-blocks, then each sub-block is modified by shorter phase sequences than that used in traditional SLM scheme. Finally, a low complexity conversion block is used to replace the conventional IFFT blocks to further reduce the complexity. To validate the efficiency of the proposed scheme, simulation results in terms of total number of complex operations, cumulative distribution function (CCDF) and bit error rate (BER) performance are carried out. The obtained results illustrate that the RC-SLM scheme outperforms the traditional SLM scheme in terms of PAPR reduction performance and achieving lower computational complexity. The effects of carrier frequency offset (CFO) on the BER performance of the proposed RC-SLM scheme is also introduced in this paper.

***Keywords:*** *Filter Bank Multi-Carrier (FBMC), Orthogonal Frequency Division Multiplexing (OFDM), peak-to-average power ratio (PAPR), selective mapping (SLM) scheme*

## 1     INTRODUCTION

Multicarrier modulations (MCM) attract more attention because of their capability to efficiently cope with frequency selective fading channels (Hassan), (Weinstein) and (Hassan, Zhu, El-Khamy, Dessouky, El-Dolil, and Abd El-Samie). Therefore, MCM has been suggested as a candidate for future communication systems. Filter Bank Multi-Carrier (FBMC) is one of the most recent modulation techniques that used in future communication systems. Compared with conventional Orthogonal Frequency Division Multiplexing (OFDM) with a Cyclic Prefix (CP-OFDM), FBMC has lower spectrum

sidelobes and therefore less sensitive to Inter-Carrier Interference (ICI) and provides good robustness to carrier frequency offset (CFO) (Abd El-Hamid et al.) and (Jirajaracheep et al.). Due to the absence of CP, FBMC can also provide good spectral efficiency than OFDM systems (Jirajaracheep et al.) and (Cheng et al.). However, FBMC likes any MCM suffers from large peak to average power ratio (PAPR) at transmitter. This large PAPR causes signal distortion and degrade BER performance. To solve this problem, there are many PAPR reduction methods presented in literature (Laabidi et al.), (Boyapati and Prema), (Chaitanya et al.) and (Zhang et al.). A common drawback of these methods is that, they are

unable to achieve good PAPR reduction without increasing computational complexity and degrading BER performance.

Selective mapping (SLM) is one of the most common PAPR reduction scheme presented in literature. The main idea of SLM scheme is to generate different transmit sequences that represent the original data and then selecting the sequence that has the smallest PAPR to transmit (Hassan et al.), (A. Devi et al.) and (Hassan, EL-Khamy et al.). However, SLM scheme has some drawbacks such as; *first*, in order to help the receiver to recover the original data from the transmitted sequences we need to transmit side information bits which reduce the spectral efficiency of the SLM-based systems. The *second* drawback is the large computational complexity resulted from using different sequences and hence different inverse fast Fourier transforms (IFFTs) blocks. To improve the spectral efficiency of the SLM-based systems, we proposed a small overhead (s-SLM) scheme in (Hassan, EL-Khamy et al.) which can combat the first drawback mentioned above.

The work in this paper will address the second drawback, which is the large computational complexity. There are many schemes presented in literature to solve the large computational complexity of PAPR reduction based on SLM scheme. Some of these techniques focuses on reducing the computational complexity using the manipulation of IFFT blocks as described in (Zhang et al.) and (Wang et al.). Another approach of complexity reduction uses coding techniques as discussed in (Jie et al.). However, these schemes achieve PAPR reduction worse than the traditional SLM scheme.

This paper proposes a new reduced complexity SLM (RC-SLM) scheme. The basic idea of the RC-SLM scheme is to divide the frequency domain data symbols into different sub-blocks, then each sub-block is modified by shorter phase sequences than that used in traditional SLM scheme. Finally, a low complexity conversion block is used to replace the conventional IFFT blocks to further reduce the complexity. The performance of the proposed RC-SLM scheme is studied with computer simulation in terms of total number of complex operations, cumulative distribution function (CCDF) and bit error rate (BER) performance are carried out. The obtained results show that the proposed RC-SLM scheme can outperform the traditional SLM scheme in terms of PAPR reduction. Moreover, its computational complexity is order of magnitude less than that of the traditional SLM scheme. The effects of carrier frequency offset (CFO) on the BER performance of the proposed RC-SLM scheme is also introduced in this paper.

The remainder of the paper is organized as follows. Section 2 presents FBMC system model using SLM scheme. The proposed scheme is presented in Section 3. Section 4, describes the complexity analysis for the proposed scheme. Simulation and analytical results and useful discussions are provided in Sections 5, followed by the conclusions in Section 6.

# 2 FBMC SYSTEM MODEL USING SLM SCHEME

## 2.1 System Model

This subsection presents the basic idea behind the Offset Quadrature Amplitude Modulation-based-FBMC (OQAM-FBMC) system. Let $X_{k,n}$, be the transmitted data samples of FBMC in time domain (TD), which is the real or imaginary part of QAM data symbol on the $k^{th}$ subcarrier during the $n^{th}$ transmitted FBMC symbol. The data symbol $a_{k,n}$ is phase adjusted using the phase term, $e^{j\varphi_{k,n}}$, where $\varphi_{k,n} = \frac{\pi}{2}(k+n)$. This is in order to achieve the orthogonality conditions of the filters and avoid interference between data symbols. The transmitted data signal $x[i]$ can be written as

$$x[i] = \sum_{k=1}^{K-1} \sum_{n \in Z} X_{k,n} g[k - nM/2] e^{j\frac{2\pi i}{M}(k-\frac{D}{2})} e^{j\varphi_{k,n}}, \qquad (1)$$

where $D$ is the delay term depending on the length of PF $g[k]$ and $K$ is the total number of subcarriers.

Due to the overlapping structure and the length of the pulse shape of OQAM-FBMC signal. It essentially suffers from high PAPR. The PAPR of the transmitted OQAM-FBMC signal in (1) can be expressed as:

$$PAPR = \frac{max|x(i)|^2}{E[|x(i)|^2]} \qquad (2)$$

where $E[x(i)]$ represent the expectation of $x(i)$. According to (2), the value of PAPR can be obtained by the ratio between the maximum envelope power (peak value) and the average power. The discrete-time signal of FBMC, $x[i]$ is obtained by sampling the time signal $x(t)$. We usually use an oversampling factor $J$ to get a good estimation of the PAPR value of the time domain signal. As shown in (Hassan), an oversampling factor of 4 is good enough to approximate the true PAPR.

The most suitable method used to evaluate the comportment of PAPR is the CCDF, since it being a random variable. The CCDF evaluate the probability that the maximum power level of a data block reaches or exceeds a given threshold value and it can be written as follows:

$$CCDF = Pr\left[PAPR > PAPR_0\right] \qquad (3)$$

## 2.2 The Basic Concept of Traditional SLM Scheme

The basic concept of traditional SLM scheme, is to form a set of different transmit data sequences, all of them represent the original data sequence. Then selecting the sequence that has the smallest PAPR to transmit (Hassan, EL-Khamy et al.). To generate these different data sequences, each data sequence is multiplied element by element by $U$ different phase sequences, each phase sequence has a length of $K$, and, $S^{(u)} = [s_{u,0}, s_{u,1}, \ldots, s_{u,K-1}]^T$ is the phase rotation vector, $u = 1, 2, \ldots, U$. Therefore, we get $U$ modified data sequences. The unmodified FBMC data sequence can be included in the modified set by using a sequence of all one vector, $S^{(1)}$ with length of $K$. The basic concept of traditional SLM scheme is presented in Fig. 1
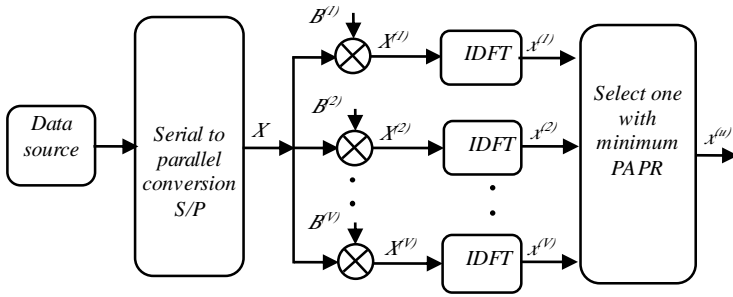


**Fig. 1.** Block diagram of the conventional SLM scheme.

The modified signal that obtained from multiplying data sequence, $X$ by phase sequences, can be written as,

$$X^{(u)} = X \cdot S^{(u)}, \qquad 1 \le u \le U \qquad (4)$$

The elements, $s_{u,k}$, $k = 0,1,\ldots K-1$, of the vector $S^{(u)}$ are chosen from the set $\{\pm1, \pm j\}$ to simplify the multiplication process. To achieve good PAPR reduction, we select the sequence $x^{(v)}$ that has the lowest PAPR from the modified data sequences. In order to help the receiver to recover the original data from the transmitted sequences, this traditional SLM scheme requires the transmission of SI bits about the selected phase sequence which reduces the spectral efficiency of the SLM-based systems. In (Hassan, EL-Khamy et al.) we tried to overcome this limitation by proposing a s-SLM scheme which can improve both spectral efficiency and BER performance. This paper focuses on another limitation of traditional SLM scheme which is very large computational complexity.

In traditional SLM scheme, the required number of IFFT operations is $U$ and it needs $N_{SI} = \lceil \log_2 U \rceil$ of SI bits for each data block sequence, with $\lceil y \rceil$ represents the smallest integer number greater than or equal to $y$. In this scheme, the amount of PAPR reduction is determined according to the value of used phase sequences $U$ and their design. In transmitting the sequence with the lowest PAPR value, the probability that the PAPR exceeds a certain value of $PAPR_0$, according to (Hassan, EL-Khamy et al.), is given by:

$$\Pr\left[PAPR_{Trad.-SLM} > PAPR_0\right] = \left[1 - (1 - e^{-PAPR_0})^K\right]^U \quad (5).$$

## 3 THE PROPOSED SCHEME

As explained above and shown in figure 1, the traditional SLM scheme uses a large number of IFFT blocks according to the number and the length of used phase sequences which increase its computational complexity. There are many works presented in literature to reduce the computational complexity of traditional SLM scheme (Zhang et al.) and (Wang et al.). However, most of these works reduce the computational complexity of SLM based schemes at the cost of degrading the PAPR reduction capability and BER performance. For example, in (Wang et al.) conversion matrices were developed to replace IFFT stages in traditional SLM scheme. Considering a FBMC system with $K$ subcarriers and $J$ oversampling factor, each conversion process in (Wang et al.) needs only $3JK$ complex additions to compute an $JK$-point IFFT which reduces the computational complexity but at the cost of degrading system performance.

To overcome the above limitation, we propose a RC-SLM scheme, which based on reducing both phase sequences length and the number of IFFT calculations. Reducing the phase sequences length can be achieved by dividing the data sequence, $X$, into $B$ sub-blocks each of length $L_s = K/B$. For each sub-block we multiply it by different phase sequences, $s^{(m)}$, with length $L_s$ which is shorter than those used in the traditional SLM scheme. Comparing the proposed scheme with the schemes presented in (Zhang et al.) and (Wang et al.), the $L_s$ point IFFT is replaced the $K$-point IFFT of the traditional SLM scheme which considerably reduces the computational complexity of the proposed scheme.

Finally, a low complexity conversion block (LCCB) is used to replace the conventional IFFT blocks to further reduce the complexity. The conversion process needs only $3JK$ complex additions to compute a $JK$-point IFFT. Therefore, in the proposed scheme, only one IFFT output can be used to produce the other candidate signals. At the final stage, we calculate the PAPR for all the modified sub-blocks, then selecting the sub-block that has the smallest PAPR for transmission. Fig. 2 presents the stages of the proposed scheme.

We named the LCCB presented in Fig. 2 as, **Replacement conversion (R),** and used instead of IFFT block in traditional SLM scheme. The main concept of this conversion can be

explained as follows; as shown in Fig. 3, the signals $x_1$ and $x_2$ are the IFFT of $X_1$ and $X_2$, respectively with $X_1 = X.\ s^{(1)}$ and $X_2 = X.\ s^{(2)}$ where $s^{(m)}$ is the $L_s$ length phase sequence. In LCCB, **R**, the output of IFFT, $x_1$ is used to obtain another IFFT output, $x_2$ as follows:

$$x_1 = \text{IFFT}\{X_1\} = WX_1 = W\ X\ s^{(1)} \tag{6}$$

$$x_2 = \text{IFFT}\{X_2\} = WX_2 = W\ X\ s^{(2)} \tag{7}$$

with $W$ represent the IFFT matrix:

$$W = \frac{1}{L_s}\begin{bmatrix} 1 & 1 & 1 & \cdots & 1 \\ 1 & W_{L_s}^1 & W_{L_s}^2 & \cdots & W_{L_s}^{L_s-1} \\ 1 & W_{L_s}^2 & W_{L_s}^4 & \cdots & W_{L_s}^{2(L_s-1)} \\ \vdots & \vdots & \vdots & \ddots & \vdots \\ 1 & W_{L_s}^{L_s-1} & W_{L_s}^{2(L_s-1)} & \cdots & W_{L_s}^{(L_s-1)(L_s-1)} \end{bmatrix} \tag{8}$$

In Eq. (8), $W_{Ls} = \exp\{j2\pi/M\}$. It clear from Eq. (8) that, the phase sequence $s^{(1)}$ is all-one vector with length $L_s$ and so the original FBMC data is included with the other modified data sequences. By substituting for $s^{(1)}$ in Eq. (6) we get:

$$x_1 = \text{IFFT}\{X_1\} = WX_1 = W\ X \tag{9}$$

Eq.(9), can be rewritten as:

$$X = W^{-1}\ x_1 \tag{10}$$

where $W^{-1}$ is the FFT matrix. Substituting from Eq. (10) into Eq. (7) we get:

$$x_2 = W\ W^{-1}\ x_1\ s^{(2)} = I_{L_s} x_1\ s^{(2)} \tag{11}$$

where $I_{Ls}$ represent the identity matrix. This analysis explains how the proposed LCCB can simplify the SLM scheme, where we can get the next output, $x_2$ by simply multiply the current output $x_1$ with identity matrix, $I_{Ls}$ then multiply the result by the next phase sequence as indicated by Eq. (11). In general, the $n$-th output is expressed as:

$$x_n = W\ W^{-1}\ x_1\ s^{(n)} = I_{L_s} x_1\ s^{(n)} \tag{12}$$

# 4    COMPLEXITY CALCULATION

The numbers of complex multiplication, $N_m$ and complex addition, $N_a$ required for $K$-point IFFT are $(K/2 \log_2 K)$ and $(K \log_2 K)$, respectively (Zhang et al.), (Alsusa and Yang). Therefore, for $U$ individual phase sequences we need $U$ IFFT operations in traditional SLM, (T-SLM). The total number of

multiplication and addition required for T-SLM scheme can be calculated as:

$$N_{m,\ \text{T-SLM}} = U \times \frac{JK}{2}\log_2 JK + U \times JK \tag{13}$$

$$N_{a,\ \text{T-SLM}} = U \times JK \log_2 JK \tag{14}$$

In T-SLM scheme, the number of multiplication of data sequence with phase sequences before IFFT stages is given in the second term in Eq. (13). As explained in Fig. 2, the proposed RC-SLM scheme requires $B$ sub-blocks, to get the phase modulated data, each sub-block requires one multiplication before IFFT stage and one IFFT stage is used for each sub-block. From Fig. 2 also we can note that, the LCCB, **R**, needs no multiplication processes and $3JL_s$ complex additions. In our case we consider $U$ phase sequences i.e., we use $U$-1 number of LCCB for each sub-block.

Now we can calculate the total number of multiplication and addition that used in our proposed RC-SLM scheme as follows:

$$N_{m,\ \text{RC-SLM}} = B \times \frac{JL_s}{2}\log_2 JL_s + B \times JL_s \tag{15}$$

$$N_{a,\ \text{RC-SLM}} = B \times JL_s \log_2 JL_s + 3B(U-1)JL_s \tag{16}$$

The computational complexity reduction ratio (CCRR) is used to compare the complexity of RC-SLM scheme with T-SLM scheme. The CCRR can be written as follows:

$$\text{CCRR} = \left(1 - \frac{\text{Proposed RC-SLM scheme complexity}}{\text{Traditional  T-SLM scheme complexity}}\right) \times 100\ \% \tag{17}$$

The number of complex operations for both RC-SLM and T-SLM schemes is shown in Fig. 4. The results in Fig. 4 are obtained using $B = 2$, $J = 4$ and $U = 4$. From this figure we can note that, RC-SLM scheme achieves much lower computational complexity than T-SLM. Numerically, at $K = 256$, RC-SLM scheme provides 45 % and 23 % reduction in number of required additions and multiplications, respectively when compared with T-SLM scheme.

Figure 5 presents the total number of complex operations for the RC-SLM scheme and the schemes presented in (Zhang et al.), (Alsusa and Yang). This figure also ensures the priority of the proposed scheme when compared to the schemes presented in literature in terms of computational complexity.

Table 1 presents the CCRR of both RC-SLM and T-SLM schemes with $B = 2$, $J = 4$, $K = 128$, $L_s = 64$ and different values of $U$. In Table 1 we consider that both schemes have equal numbers of candidates. The data presented in Table 1 indicate

that the number of multiplications in RC-SLM scheme is constant despite the change of *U*. In addition, the RC-SLM scheme computational complexity is reduced rapidly by increasing the value of *U*.
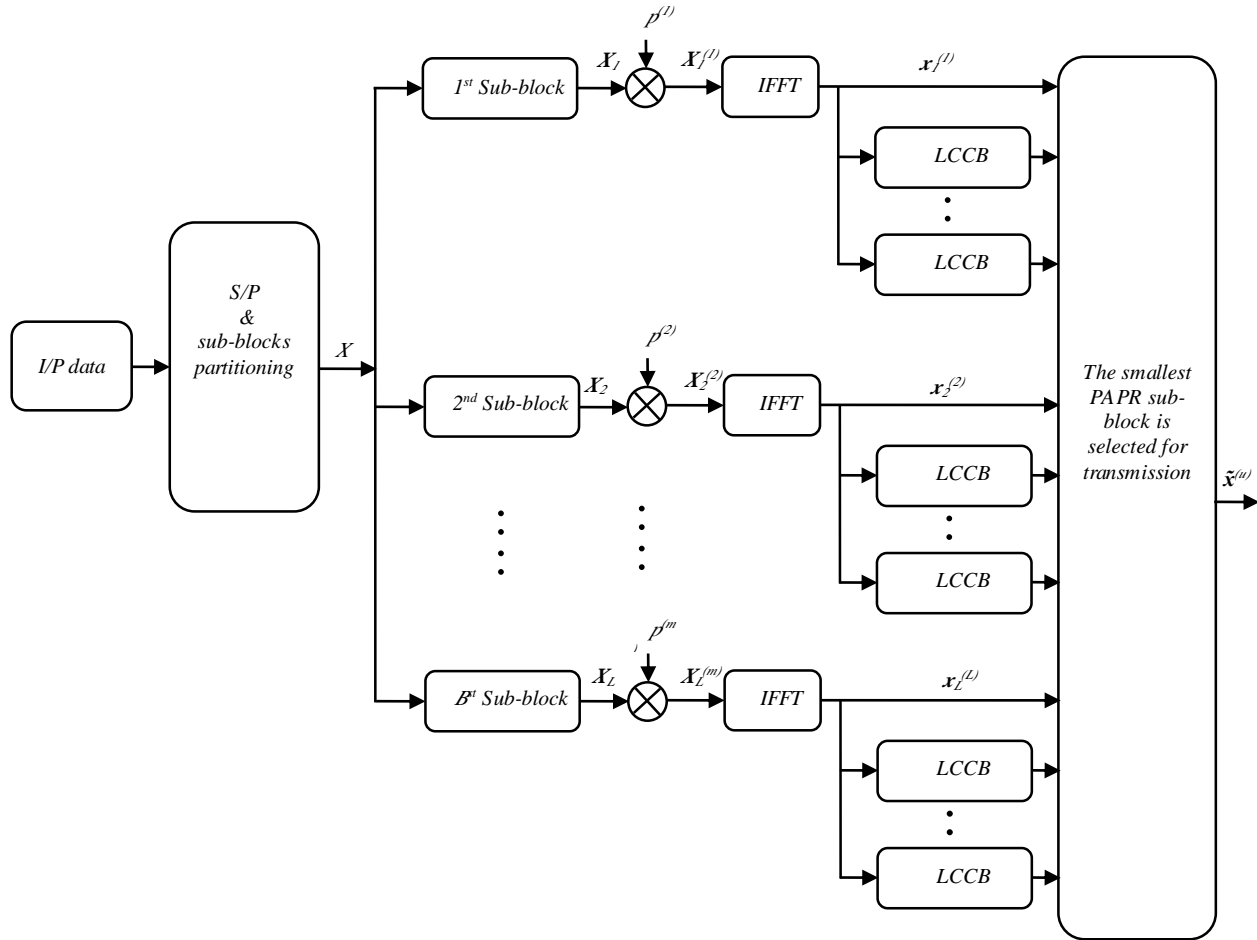


**Fig. 2.** The proposed RC-SLM scheme block diagram.
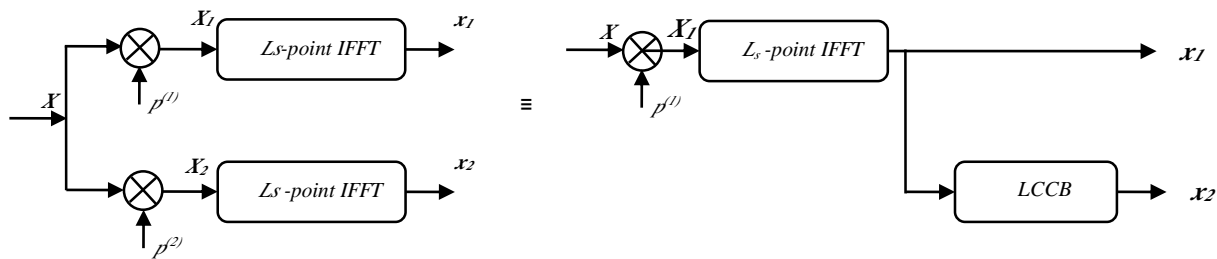


**Fig. 3.** The conversion replacement for IFFT computation.

**Table 1:** *The CCRR of both RC-SLM and T-SLM schemes in terms of U.*

| *U* | Number of multiplications, $N_m$ | | CCRR | Number of additions, $N_a$ | | CCRR |
|---|---|---|---|---|---|---|
| | T-SLM | RC-SLM | | T-SLM | RC-SLM | |
| **2** | 5632 | 2560 | 54.6 % | 9216 | 5632 | **39 %** |
| **4** | 11264 | 2560 | 77.3 % | 18432 | 8704 | **52.8 %** |
| **8** | 22528 | 2560 | 88.9 % | 36864 | 14848 | **60%** |

**Table 2:** *The CCRR of both RC-SLM and T-SLM schemes in terms of B.*

| B | Number of multiplications, $N_m$ | | CCRR | Number of additions, $N_a$ | | CCRR |
|---|---|---|---|---|---|---|
| | T-SLM | RC-SLM | | T-SLM | RC-SLM | |
| 2 | 11264 | 2560 | 77.3 % | 18432 | 8704 | 53 % |
| 4 | 11264 | 5120 | 54.5 % | 18432 | 17408 | 6 % |

**Table 3:** *The CCRR of both RC-SLM scheme and C-DSLM scheme in terms of U.*

| U | Number of multiplications, $N_m$ | | CCRR | Number of additions, $N_a$ | | CCRR |
|---|---|---|---|---|---|---|
| | C-DSLM | RC-SLM | | C-DSLM | RC-SLM | |
| 2 | 147456 | 2560 | 98.2 % | 393216 | 5632 | 98.6 % |
| 4 | 147456 | 2560 | 98.2 % | 589824 | 8704 | 98.5 % |
| 8 | 147456 | 2560 | 98.2 % | 983040 | 14848 | 98.5 % |
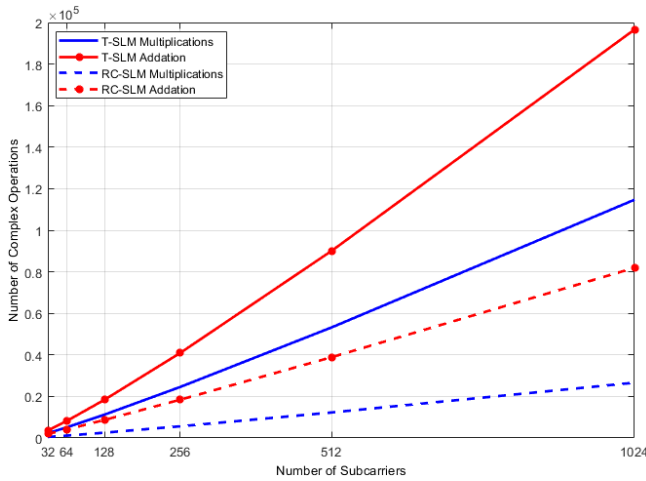


**Fig. 4.** The number of complex operations for both RC-SLM and T-SLM schemes.



**Fig. 5**. The total number of complex operations for RC-SLM scheme and the schemes presented in (Wang et al.) and (Alsusa and Yang).

Now we consider the effects of changing the values of *B* on the value of CCRR for both schemes using $J = 4$, $K = 128$, and $U = 4$ as shown in Table 2. This table also indicate that the computational complexity of the RC-SLM scheme is smaller than that of the T-SLM scheme even for large values of *B*.

One of the recent low-complexity SLM scheme for PAPR reduction in FBMC presented in literature is the conversion vector-based low-complexity dispersive selection mapping (C-DSLM) scheme (Cheng et al.). The total number of multiplication and addition of C-DSLM was presented in Table 2 in (Cheng et al.). The CCRR comparison between RC-SLM scheme and C-DSLM scheme is presented in Table 3 when $J = 4$, $K = 128$, $B = 2$, and $L_s = 64$.

The values of CCRR presented in the above tables show the effectiveness of the proposed scheme in term of computational complexity over the schemes presented in (Alsusa and Yang) and (Cheng et al.).

## 5       SIMULATION RESULTS

In this section, we provide theoretical and simulation results of CCDF and BER, to investigate the performance of the proposed RC-SLM scheme. The obtained results are compared with those of the existing PAPR reduction schemes in literature and with the T-SLM. During simulation we used an FBMC system with $K = 128$ subcarriers, $J = 4$ and bandwidth of 20 MHz. The elements of phase rotation vectors used to form the modified data sequences are generated randomly, where its elements are selected randomly from the set $\{\pm 1, \pm j\}$. For the considered schemes we use the same number of candidates while changing both $U$ (no. of phase sequences) and $B$ (no. of sub-blocks) during the simulations.
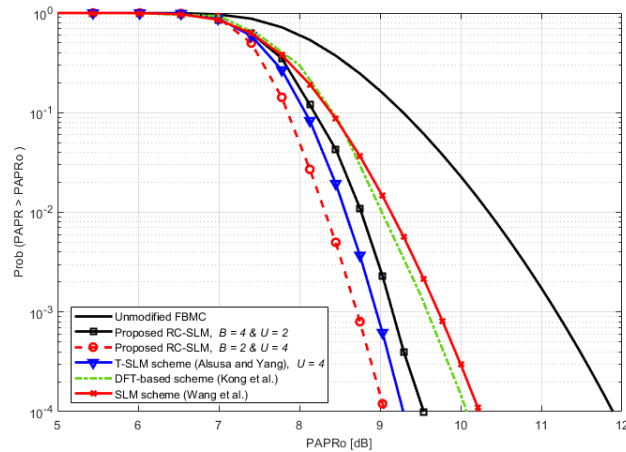


**Fig. 6**. CCDF of RC-SLM scheme using different values of $B$ and $U$.

Figure 6 presents the CCDF of RC-SLM scheme using different values of $B$ and $U$. For comparison, the CCDF of unmodified FBMC signal, SLM scheme (Wang et al.), T-SLM scheme (Alsusa and Yang) and discrete Fourier transform (DFT)-based scheme proposed in (Kong et al.) using $B = 2$ are also presented. According to the obtained results, for more candidates, i.e., the case with $U = 4$ and $B = 2$, the proposed RC-SLM scheme provides good PAPR reduction than the case with $U = 2$ and $B = 4$. Therefore, the following results are obtained with $U = 4$ and $B = 2$. From Fig. 6 we can note that, the proposed scheme also outperforms the other in terms of PAPR reduction.

As in T-SLM scheme, the RC-SLM scheme sends SI bits to the receiver to correctly recover the transmitted data. In (Hassan, EL-Khamy et al.) we proposed a s-SLM scheme that enhances the probability of detection of these SI bits. Hence the BER performance can improved accordingly. In this work, we can apply the same manner to enhance the correct detection of the SI bits.

Figure 7 provides a performance comparison between both RC-SLM and T-SLM (Alsusa and Yang) using different values of $U$ and with $B = 2$. The obtained results showed that, the RC-SLM scheme provides good CCDF than T-SLM. Numerically, at CCDF of $10^{-3}$ and $U = 8$, the proposed scheme achieves 0.32 dB improvements in PAPR reduction over the T-SLM scheme. Unlike the low complexity schemes presented in (Zhang et al.) and (Wang et al.) and (Wang and Li), which provide small complexity but at the cost of increasing PAPR value. Therefore, the proposed scheme can provide both small computational complexity and reducing the value of PAPR as compared to [(Wang et al.), (Alsusa and Yang) and (Kong et al.). As explained above, the BER of the proposed scheme can be improved by applying the same concept presented in (Hassan, EL-Khamy et al.).
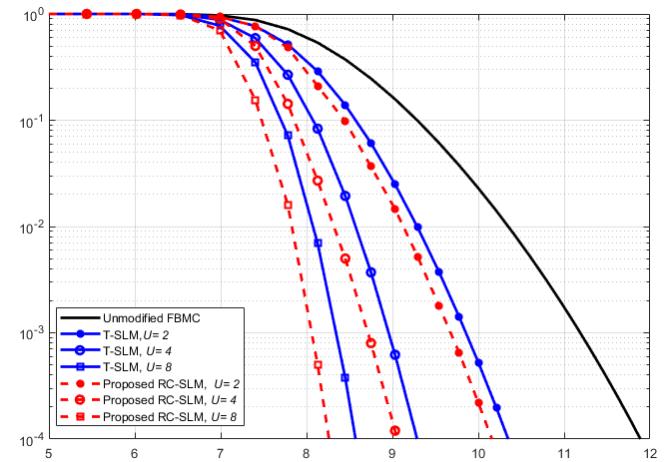


**Fig. 7.** CCDFs of RC-SLM scheme using $B = 2$, T-SLM and DFT-based schemes.

Figure 8 presents a BER comparison between the unmodified FBMC, DFT-based scheme and the proposed RC-SLM scheme using $B = 2$ over Rayleigh fading channel. Due to the phase rotation vectors in the proposed RC-SLM scheme, there is a slight degradation in its BER performance when compared with unmodified FBMC scheme. For example, at BER of $10^{-3}$, the proposed RC-SLM scheme requires 2.48 dB more signal-to-noise ratio (SNR) to achieve the same BER performance of unmodified FBMC scheme. On the other hand, the proposed RC-SLM scheme achieves nearly the same BER performance as DFT-based scheme (Kong et al.). This slight

degradation in BER performance comes with the good improvement in PAPR reduction of the proposed scheme and its lower computational complexity as compared to the other schemes presented in this paper.

One of the common problems in wireless communications is the carrier frequency offset (CFO), which results due to imperfect synchronization between transmitter and receiver oscillators, or the Doppler effect (Abd El-Hamid et al.), (Singh et al.) and (Rugini, Banelli). CFO causes a loss of subcarriers orthogonality which results in rising the intercarrier interference (ICI) and therefore, performance degradation.

Let ε represents the normalized CFO, Eq. (18) indicates the effect of CFO on the received signal $y[n]$,

$$y[n] = (x[n] * h[n])e^{\frac{-j2\pi n\varepsilon}{N}} + w[n] \qquad (18)$$

where $x[n]$ is the transmitted signal, $h[n]$ is the discrete impulse response of the fading channel, $w[n]$ is the Additive White Gaussian Noise (AWGN) and $(*)$ denotes the convolution operation.
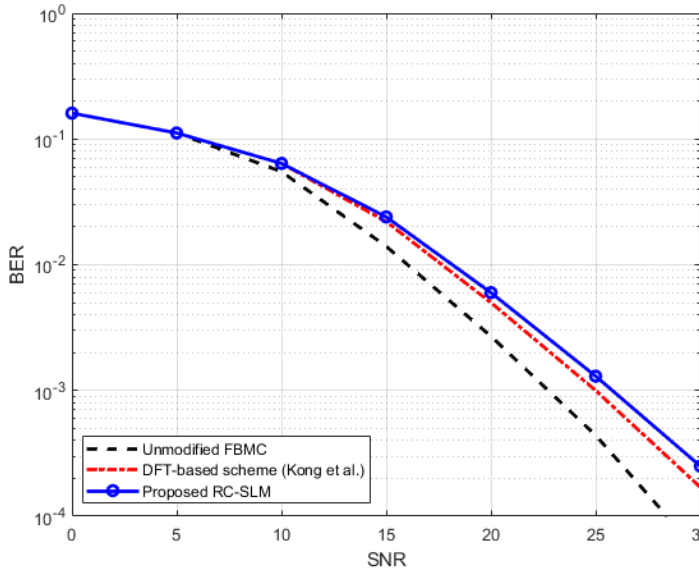


**Fig. 8.** BER performance of the unmodified FBMC, proposed RC-SLM scheme using $L = 2$ and DFT-based schemes over Rayleigh fading channel.
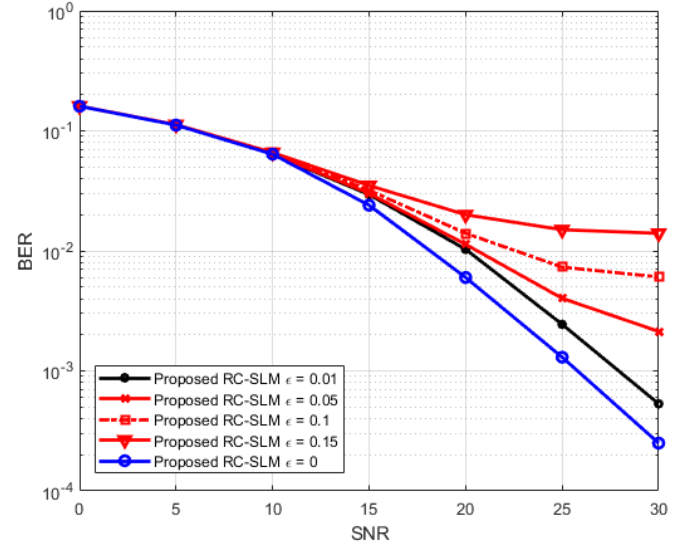


**Fig. 9.** Effects of CFO on the BER performance of the proposed RC-SLM scheme over Rayleigh fading channel.

The effects of CFO on the BER performance of the proposed RC-SLM scheme over Rayleigh fading channel is shown in Fig. 9 for different values of ε. It is clear from this figure that, increasing the values of ε, will degrade the BER performance, this performance degradation is due to ICI which rises as the value of ε increase.

# 6    CONCLUSION

This paper presented a new RC-SLM scheme that reduces the computational complexity of traditional SLM schemes and providing distinctive PAPR reduction. The main idea of the proposed scheme is to shortening the length of data sequence by dividing it into several sub-blocks, then each sub-block was modified by shorter phase sequences. Finally, a new low complexity conversion block was proposed to replace the conventional IFFT blocks to further reduce the complexity. Computer simulation was used to validate the effectiveness of the proposed scheme. The obtained results showed that the proposed RC-SLM scheme was be able to achieve the lowest computational complexity when compared with the other low complexity schemes proposed in the literature while at the same time improves the PAPR reduction performance. Numerically, at $K = 256$, RC-SLM scheme provides 45 % and 23 % reduction in number of required additions and multiplications, respectively when compared with traditional SLM scheme. The obtained results also showed that, the RC-SLM scheme provides good CCDF than traditional SLM. Numerically, at CCDF of $10^{-3}$ and $U = 8$, the proposed scheme achieves 0.32 dB improvements in PAPR reduction over traditional SLM scheme. Finally, the BER performance

degradation due to the presence of CFO was discussed also in this paper.

## 7    REFERENCES

[1] Hassan, Emad. Multi-carrier communication systems with examples in MATLAB: A new perspective. CRC Press, 2016.

[2] Weinstein, Stephen B. "The history of orthogonal frequency-division multiplexing [History of Communications]." IEEE Communications Magazine 47.11 (2009): 26-35.

[3] Hassan, Emad S., et al. "Performance evaluation of OFDM and single-carrier systems using frequency domain equalization and phase modulation." International Journal of Communication Systems 24.1 (2011): 1-13.

[4] Abd El-Hamid, Zahraa, et al. "New multiple-input multiple-output-based filter bank multicarrier structure for cognitive radio networks." IET Communications 13.10 (2019): 1514-1523.

[5] Jirajaracheep, Panya, Tanairat Mata, and Pisit Boonsrimuang. "PAPR reduction in FBMC-OQAM systems using trellis-based D-SLM with ABC algorithm." 2020 17th International Conference on Electrical Engineering/Electronics, Computer, Telecommunications and Information Technology (ECTI-CON). IEEE, 2020.

[6] Cheng, Xing, et al. "A novel conversion vector-based low-complexity SLM scheme for PAPR reduction in FBMC/OQAM systems." IEEE Transactions on Broadcasting 66.3 (2020): 656-666.

[7] Laabidi, Mounira, Rafik Zayani, and Ridha Bouallegue. "A novel multi-block selective mapping scheme for PAPR reduction in FBMC/OQAM systems." 2015 World Congress on Information Technology and Computer Applications (WCITCA). IEEE, 2015.

[8] Boyapati, Ujjwala, and S. Chris Prema. "Reduction of PAPR in FBMC: A Comparative Analysis." 2018 IEEE Recent Advances in Intelligent Computational Systems (RAICS). IEEE, 2018.

[9] Bulusu, SS Krishna Chaitanya, et al. "Reduction of PAPR for FBMC-OQAM systems using dispersive SLM technique." 2014 11th international symposium on wireless communications systems (ISWCS). IEEE, 2014.

[10] Yang, Chaosan, et al. "Modified SLM scheme of FBMC signal in satellite communications." IET Communications 13.11 (2019): 1702-1708.

[11] Hassan, Emad S., et al. "A Simple Selective Mapping Algorithm for the Peak to Average Power Ratio in Space Time Block Coded MIMO-OFDM Systems." HPCNCS. 2008.

[12] D Devi, A., et al. "A Phase Offset Selective Mapping Technique for PAPR Reduction in MIMO-UFMC." 2021 Fifth International Conference on I-SMAC (IoT in Social, Mobile, Analytics and Cloud)(I-SMAC). IEEE, 2021.

[13] Hassan, Emad S., et al. "Peak-to-average power ratio reduction in space–time block coded multi-input multi-output orthogonal frequency division multiplexing systems using a small overhead selective mapping scheme." IET communications 3.10 (2009): 1667-1674.

[14] Zhang, Si-Yu, and Behnam Shahrrava. "A SLM scheme for PAPR reduction in polar coded OFDM-IM systems without using side information." IEEE Transactions on Broadcasting 67.2 (2020): 463-472.

[15] Wang, Chin-Liang, and Yuan Ouyang. "Low-complexity selected mapping schemes for peak-to-average power ratio reduction in OFDM systems." IEEE Transactions on signal processing 53.12 (2005): 4652-4660.

[16] Yang, Jie, Lei Chen, and Wei Mao. "A modified selected mapping technique to reduce the peak-to-average power ratio of OFDM signal." 2007 Digest of Technical Papers International Conference on Consumer Electronics. IEEE, 2007.

[17] Alsusa, Emad, and Lin Yang. "Selective post-IFFT amplitude randomising for peak-to-average power ratio reduction in orthogonal frequency-division multiplexing-based systems." IET communications 2.4 (2008): 553-561.

[18] Wang, Sen-Hung, and Chih-Peng Li. "A low-complexity PAPR reduction scheme for SFBC MIMO-OFDM systems." IEEE Signal Processing Letters 16.11 (2009): 941-944.

[19] Cheng, Xing, et al. "A novel conversion vector-based low-complexity SLM scheme for PAPR reduction in FBMC/OQAM systems." IEEE Transactions on Broadcasting 66.3 (2020): 656-666.

[20] Kong, Dejin, et al. "A novel DFT-based scheme for PAPR reduction in FBMC/OQAM systems." IEEE Wireless Communications Letters 10.1 (2020): 161-165.

[21] Singh, Daljeet, et al. "Symbol error rate analysis of OFDM system with CFO over TWDP fading channel." Wireless Personal Communications 109.4 (2019): 2187-2198.

# DOUBLY FED INDUCTION GENERATOR AS A SYNCHRONOUS GENERATOR BY EXPERIMENT

**Ahmed S. Oshaba[1], Dina S. M. Osheba[2], Mervet A. Shanab[2]**

[1] Department of Electrical Engineering, College of Engineering, Jazan University, Jizan 45142, Saudi Arabia;
[2] Department of Electrical Engineering, Menoufiya University, Shebin El-kom 32511, Egypt

**\*Corresponding author**:

*Ahmed S. Oshaba*

   **Email address:**

aoshaba@jazanu.edu.sa

Recently, Doubly Fed Induction Generator (DFIG) is one of the most common machines in wind energy systems. This mainly is due to its most remarkable feature which is the variable speed constant frequency operation. Much research work has been paid in DFIG. However, most of these papers, which study the different control strategies of DFIG, deal with the machine as a set of dynamic equations without realizing the principle of its operation. The present work adopts a special insight into understanding the principle of DFIG operation. This insight is that the DFIG can be viewed as a synchronous generator. The same idea has been adopted in few papers; however, their work is based on theoretical analysis and lacks of experimental verification. Here, the present work support and enhance this idea by experimental study. An experimental setup has been built and tested to examine the performance characteristics of DFIG at different operating conditions. The results reveal that the output power of DFIG depends on the power angle (δ) which stands for the rotor voltage angle. Besides, the machine has the characteristic of (V-curves) that belongs to the synchronous machine. Hence, the DFIG behaves like the synchronous generator.

*Keywords:* Doubly Fed Induction Generator, wind energy systems, synchronous generator.

## 1.    INTRODUCTION

Due to the increasing demand of electrical energy and for clean environment, many countries all over the world work to exploit the renewable energy sources. Among these renewable sources is the wind energy. A variety of electrical generators have been employed in wind energy systems. Each of them has its merits and demerits. However, Doubly Fed Induction Generator (DFIG) remains the most popular machine in wind energy systems due to its inherent merits. The principal merit of this machine is the constant magnitude and frequency of the generated voltage despite the rotor speed variation. As a result, DFIG is always synchronized with the grid and can be directly connected with it at any time. Moreover, the rotor speed can be controlled to extract the maximum power from the wind turbine at different wind speeds. This is described by the Maximum Power Point Tracking (MPPT) control [1,2,3].

DFIG is basically a wound rotor induction machine. Its stator is directly connected to the grid, while the rotor is connected via a power electronic converter. This converter has reduced capacity and cost because only the slip power is handled in the rotor. Besides, both the active and reactive power can be controlled; consequently, the power factor is also controlled. The active power is mainly delivered to the grid throughout the stator terminals. While, throughout the rotor, the active power is exchanged in both directions according to the rotor speed. For sub-synchronous rotor speeds, the rotor borrows the active power from the grid, while for super-synchronous rotor speeds; the rotor delivers the active power to the grid [4].

The concept of considering the DFIG as asynchronous/synchronous machine has been adopted in

[5]. Typically, DFIG keeps on the induction machine features due to the slip. However, it can also be viewed as a synchronous machine since the active power depends on the angle of injected rotor voltage ($\delta$). The authors, throughout the paper, perform the analogy of DFIG with the synchronous machine based on the mathematical analysis only. Hence, their work lacks of experimental verification.

Throughout [6,21], the steady state performance characteristics of DFIG have been studied. Based on the theoretical analysis the effect of changing the magnitude and the angle of rotor voltage on the active and reactive power has been investigated. However, the results need also to be proved experimentally.

Slip control of DFIG based on PWM technique has been proposed in [7,22]. To maintain the magnitude and the frequency of the stator voltage constant with speed variation, the power converter in the rotor is controlled based on the ratio (voltage/frequency=constant). However, the test is performed with connecting the stator to a resistive load not to the grid.

Recently, several control strategies have been proposed for DFIG. The sensorless field-oriented control of DFIG has been presented as in [8,9,10,11,23]. It is used to achieve the independent control of the active and reactive power based on the current control loop. However, it is affected by the change of the machine internal parameters. Throughout [12,13,24], vector control based on fuzzy logic controllers has been proposed. Compared to PI controller, fuzzy logic controller is robust and simple in controlling the nonlinear and complex systems. Moreover, vector control based adaptive sliding mode controller has been described as in [14,15]. Adaptive sliding mode control is effective for the nonlinear systems since it is distinguished by fast convergence and high tracking accuracy. Throughout [16], vector control based on rotor current sensorless control has been proposed. The rotor current regulators are replaced by the stator current regulators in order to provide the decoupled control of active and reactive power. Certain control strategies of both grid side and rotor side converters, based on vector control, have been suggested in [17]. For power factor adjustment, the grid side converter is controlled based on grid voltage orientation. While, for independent control of active and reactive power, the rotor side converter is controlled based stator flux orientation.

Throughout [18,19,25], direct power control for DFIG has been introduced. It eliminates the current control loop employed in vector control method and directly regulates the active and reactive power. In addition, its dependence on the machine parameters is reduced. A certain control method to improve the voltage at the load bus based on DFIG has been proposed in [20]. This method depends on adjusting the reactive power based on controlling the rotor side d-axis voltage.

All the latter papers, which discussed the different control strategies of DFIG, depend on the dynamic equations of induction machine, in the two-phase stationary reference frame, to design the control scheme. Hence, there is a missing loop in understanding the principle of DFIG operation. To find this missing loop, this paper studies the performance characteristics of DFIG adopting the idea of DFIG analogy with the synchronous machine. This idea has been investigated theoretically throughout the previous work. Here, the experimental verification of this idea is accomplished throughout this work. An experimental setup is established in the laboratory to investigate the DFIG performance at different operating conditions.

## 2. PRINCIPLE OF OPERATION OF DFIG

As mentioned before, the remarkable feature of using DFIG in wind energy systems is obtaining a three phase AC voltage of constant magnitude and frequency as the same of the grid despite the wind speed fluctuations. Hence, the DFIG is always synchronized with the grid and can be easily connected to it at any time. Fig. 1 illustrates a schematic diagram of DFIG employed in wind energy system. Based on the variable frequency converter, which consists of the AC/DC and DC/AC converters connected between the rotor terminals and the grid, the constant magnitude and frequency of the stator voltage can be obtained. The stator voltage frequency ($F_1$) can be calculated as described by (1):

$$F_1 = \frac{PN_r}{60} \pm F_2 \tag{1}$$

Where $N_r$ is the rotor speed in (rpm), $F_2$ is the rotor voltage frequency and $P$ is the number of pair poles of DFIM. Based on (1), to maintain $F_1$ constant at the grid frequency, $F_2$ should be changed continually to face any variation of the rotor speed ($N_r$) caused by the wind. When the wind speed results in the rotation of the rotor with a speed below the nominal synchronous speed, the rotor frequency should be increased with the positive sign. This necessitates the rotation of the rotating field in the rotor in the same direction of the rotor rotation. In other words, when the rotor rotates with a speed higher than the nominal synchronous speed, the rotor frequency should be increased but with the negative sign. This requires the rotation of the rotor magnetic field in the opposite direction of the rotor rotation. Eventually, any difference of the rotor speed from the nominal synchronous speed is compensated by changing the rotor frequency. Accordingly, the rotor flux always cuts the stator windings with a constant speed that corresponds to the grid frequency.

To obtain the constant magnitude of the stator voltage that equal to the grid voltage, the rotor magnetic flux should be maintained constant. This can be achieved by operating the frequency converter, which supplies the rotor windings, based on the constant ratio (voltage /frequency=constant).
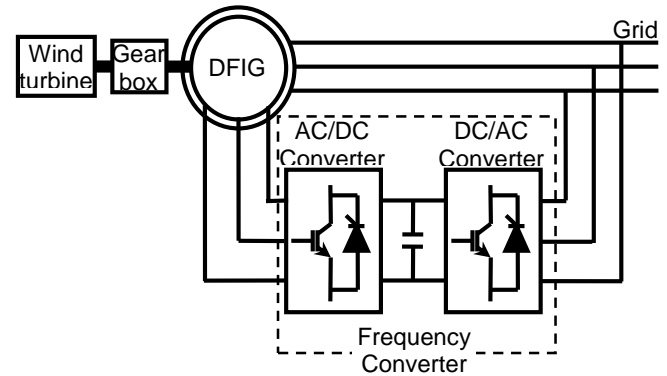


Fig. 1. A schematic diagram of DFIG-wind energy system

## 3. THE ANALOGY WITH THE SYNCHRONOUS MACHINE

From the basic principles of induction machine, the equivalent circuit per phase of doubly fed induction machine is shown in Fig. 2 (a). By considering the motoring operation mode, the stator is supplied directly from the source by a three phase AC voltage of frequency ($F_1$) equal to the grid frequency. Its value per phase is $V_1$. On the other hand, the frequency converter injects the rotor by a three phase AC voltage. Its value per phase is $V_2$, its angle is $\delta$, and its frequency is $F_2$, which is called the slip frequency since it is calculated from the following equation:

$$F_2 = SF_1 \tag{2}$$

Where $S$ is the slip. In the stator circuit, at the supply frequency, $E_1$ denotes the induced EMF in the stator windings per phase, $I_1$ is the stator phase current, $X_1$ is the stator phase leakage reactance and $R_1$ is the stator phase resistance. In the rotor circuit, at the slip frequency, $E_2$ is the induced EMF in the rotor windings per phase, $I_2$ is the rotor phase current, $X_2$ is the rotor phase leakage reactance and $R_2$ is the rotor phase resistance.

The rotor circuit is then referred to the stator side at the supply frequency resulting in the equivalent circuit illustrated in Fig. 2 (b). In this circuit, the rotor leakage reactance is modified to be $'X_{20}$ at the supply frequency. Accordingly, the rotor resistance is also modified to be $'R_2/S$ and the rotor voltage becomes $'V_2/S$. $X_m$ is the magnetizing reactance per phase at the supply frequency.

To make the analogy with the synchronous machine, the equivalent circuit shown in Fig. 2 (b) is approximated to become as in Fig. 2 (c) as described in [5]. In this circuit, the magnetizing reactance ($X_m$) is considered very large to be virtually open circuit. The equivalent resistance ($R$) and equivalent reactance ($X$) are defined by:

$$R = R_1 + \frac{'R_2}{S} \tag{3}$$

$$X = X_1 + 'X_{20} \tag{4}$$

Accordingly, the stator current can be easily computed. Hence, the stator power ($P_1$) is the real part of the multiplication of the stator voltage and stator current vectors multiplied by 3. It is expressed as:

$$P_1 = -3 \frac{\left( X \frac{V_2}{S} \sin\delta - R\left(V_1 - \frac{V_2}{S}\cos\delta\right)\right)}{R^2 + X^2} V_1 \tag{5}$$

The negative sign indicates the operation of doubly fed induction machine in generating mode.
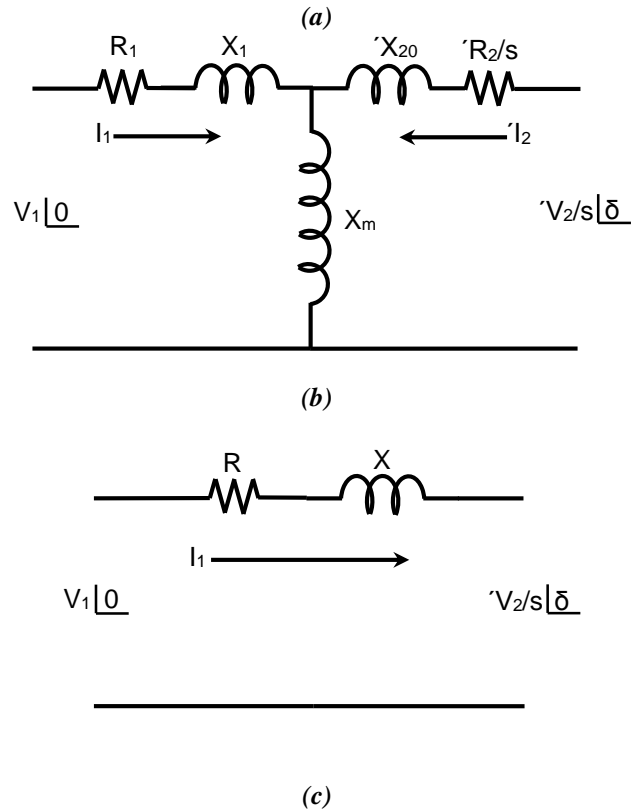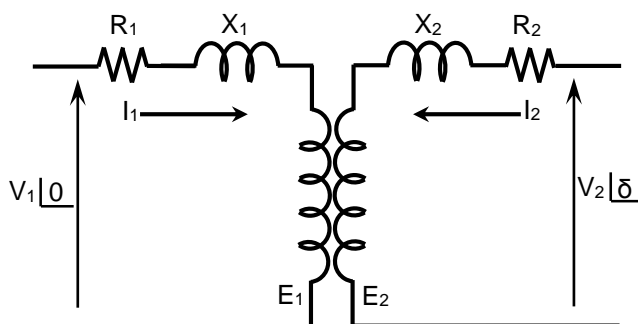






**Fig. 3.** *The equivalent circuit per phase of doubly fed induction machine*

By neglecting the equivalent resistance ($R$), the power equation resembles its relevant in synchronous machine and becomes as:

$$P_1 = -3 \frac{V_1 \left(\frac{V_2}{S}\right)}{X} \sin\delta \tag{6}$$

Accordingly, the angle of injected rotor voltage ($\delta$) represents the power angle of DFIG based on the analogy with the synchronous machine.

## 4. THEORETICAL RESULTS AND DISCUSSION

A computer program has been established based on the previous mathematical model to study the steady state characteristics of DFIM. Mainly, the results can be divided into three groups as following:

The first group of theoretical results are computed at a constant stator voltage ($V_1$=210 V) with different rotor frequencies ($F_2$= 20, 30, and 40 HZ). Fig. 4 shows the variation of stator current with rotor current at different rotor frequencies. It seems obviously that the behavior of these curves is similar to the (V-curves) of synchronous motor and the stator current approximately increases by raising the rotor frequency. The torque–speed characteristics of DFIM at different rotor frequencies are investigated as shown in Fig. 5. It is observed that the motor speed does not change with the load torque variation. However, it varies with the rotor frequency based on (1). Hence, the motor speed is synchronized with the rotor frequency. In addition, the DFIM develops a synchronous

torque in steady state.

The second group of theoretical results incorporates the DFIM characteristics under stator voltage variation with a constant rotor frequency ($F_2$=15 HZ). The variation of stator current with rotor current at different levels of stator voltage is demonstrated in Fig. 6. It also varies in the form of (V-curves) of synchronous motor. Typically, the stator current increases by raising the stator voltage. Fig. 7 exhibits the torque–speed curve of DFIM at different levels of stator voltage. It is clear that changing the stator voltage doesn't affect the motor speed.

The effect of rotor voltage variation on the motor characteristics is investigated throughout the third group of theoretical results. The rotor frequency is also constant at ($F_2$=15 Hz) and the stator voltage is constant at ($V_I$=210 V). The variation of stator current with rotor current at different levels of rotor voltage takes the behavior of (V-curves) as clear in Fig. 8. It is observed that the stator current is inversely proportional to the rotor voltage. In addition, the torque–speed curve of DFIM does not influenced by the rotor voltage variation as evident by Fig. 9

## 4.1 Experimental Verification

The experimental setup for DFIG system has been established and tested in the laboratory. The machine under test is a wound rotor induction machine representing the DFIG. It has a rating of (0.3kw, 2.2A, 230/400V, 1395 rpm, 4 poles). Its stator is directly connected to the grid which has a frequency of 50 HZ. In other words, the rotor is connected to the grid via the variable frequency converter whose frequency is adjusted manually from its panel. The converter operation is based on the constant ratio (voltage /frequency=constant). A DC motor is selected to be the prime mover since its speed can be changed easily by adjusting the armature voltage.  Fig. 3 illustrates a photo picture of the DFIG under test coupled with the DC motor.
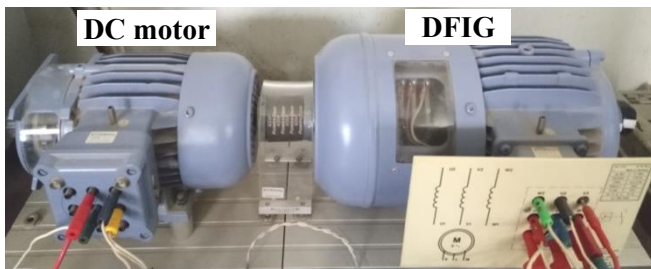


**Fig. 3**. *A photo picture of experimental DFIG coupled with a DC motor*

## 4.2 Characteristic Curves of DFIG

The first group of experimental results incorporates the curves of rotor current, stator power, and rotor power variation against the stator current which proportions to the loading. These results are recorded at a constant stator voltage ($V_I$=220 V), which equal to the grid voltage, with different rotor frequencies ($F_2$= 20, 30, and 40 HZ). These frequencies correspond the rotor speeds (900, 600, and 300 rpm) respectively. Fig. 4 shows the variation of rotor current with stator current at different rotor frequencies. It seems obviously that the behavior of these curves is similar to the (V-curves) of synchronous generator. In addition, the rotor

current increases by raising the rotor frequency. The variation of the stator power with the stator current at different rotor frequencies is illustrated in Fig. 5. It is observed that the stator power increases with increasing both the stator current and rotor frequency, but in the negative direction. Typically, this negative sign means that the stator power is delivered to grid. On the hand, the rotor power increases also by increasing both the stator current and rotor frequency, but in the positive direction as demonstrated by Fig 6. Hence, this power is supplied to the rotor since the DFIG is operated in sub-synchronous mode.
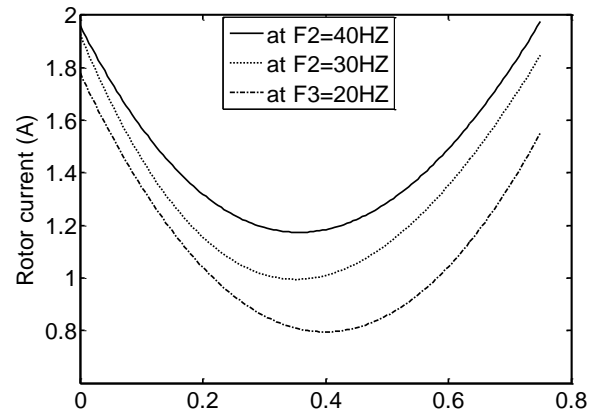


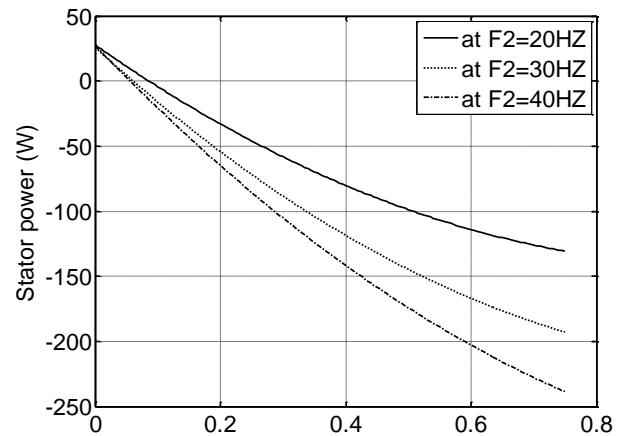**Fig. 4**. *Variation of rotor current with stator current at different rotor frequencies*



**Fig. 5**. *Variation of stator power with stator current at different rotor frequencies*
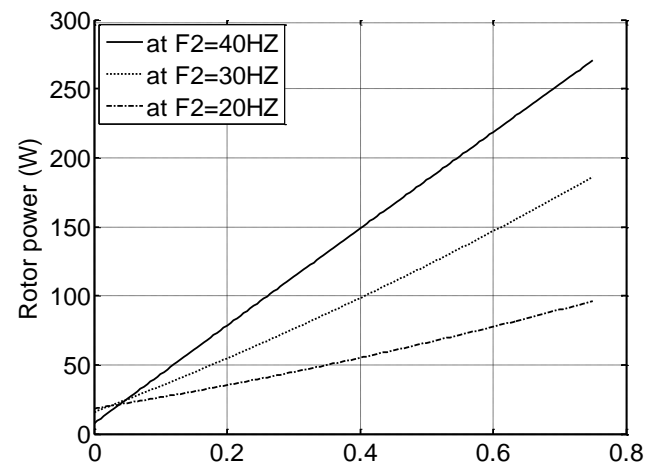


**Fig. 6**. *Variation of rotor power with stator current at different rotor frequencies*

### 4.3 Voltage and Current Waveforms of DFIG

The experimental results can be divided into four groups. The first group is recorded at a constant stator voltage ($V_1$=210 V) with different rotor frequencies ($F_2$= 10, 15, and 20 HZ). Fig. 7 shows the rotor voltage with rotor current at different rotor frequencies. It is observed that the rotor voltage (V2) does not change with the rotor current. However, it changes in proportional to the rotor frequency (F2) according to the converter ratio (V2/ F2 =constant). Besides, the motor speed is also constant with the load torque variation, but changes with the rotor frequency as indicated by Fig. 7. This confirms that the DFIM has the same torque–speed characteristic of synchronous motor. The variation of stator current with rotor current, at different rotor frequencies, is recorded as illustrated by Fig. 7. It enhances the behavior of (V-curves) of synchronous motor.

To examine the effect of changing the stator voltage on the motor characteristics, the second group of experimental results are measured at a specific rotor frequency (F2=15 Hz) and different values of stator voltage. The motor speed is also constant at a value of (1050 rpm) that corresponds the rotor frequency (F2=15 Hz) and does not influenced by the stator voltage or load torque variation as evident by Fig. 8. In other words, the stator current changes with the rotor current, at different values of stator voltage, in the manner of (V-curves) as demonstrated by Fig. 8. It is observed that the stator current decreases by reducing the stator voltage at low values of rotor current whereas, with the rotor current increase, the curves of stator current are convergent.

The third group of experimental results studies the effect of rotor voltage variation on the motor characteristics at a constant rotor frequency (F2=15 HZ). In spite of the rotor voltage and load torque variation, the motor speed is held constant at the value of (1050 rpm), corresponding to the rotor frequency (F2=15 HZ), as evident by Fig. 9. The variation of the stator current with rotor current under rotor voltage variation is determined as illustrated in Fig. 9. It is observed that by reducing the rotor voltage, the stator current increases over a wide range of rotor current variation.

To examine the effect of rotor current variation on the power factor of DFIM, the waveforms of stator phase voltage and current are recorded at different values of rotor current throughout the fourth group of experimental results. These waveforms are recorded at (V1=180V and F2=15 HZ). Fig. 9 shows the waveforms of stator phase voltage and current at a rotor current of (I2= 0.8 A). It is observed that the stator current lags the phase voltage. By increasing the rotor current to a value (I2= 1.5 A), the power factor becomes unity and the two waveforms are in phase as depicted in Fig. 9. With going on increasing the rotor current till a value (I2= 2.8 A), a leading power factor is obtained since the stator current leads the phase voltage as evident by Fig. 9. Note that the voltage waveform should be multiplied by a factor (10) and the current waveform should be divided by a factor (50) in all waveform figures.

The power factor variation of DFIM by changing the rotor current enhances the operation of DFIM as a synchronous motor.
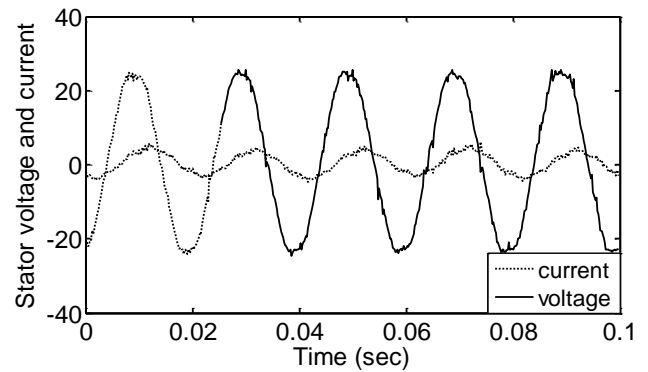


**Fig. 7.** *Waveforms of stator phase voltage and current of DFIM at ($I_2$=0.8A)*
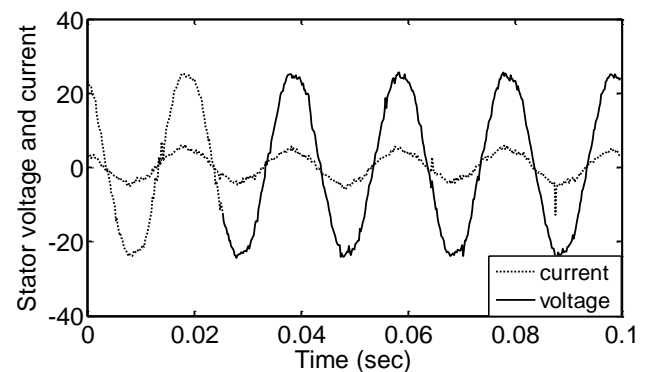


**Fig. 8.** *Waveforms of stator phase voltage and current of DFIM at ($I_2$=1.5A)*
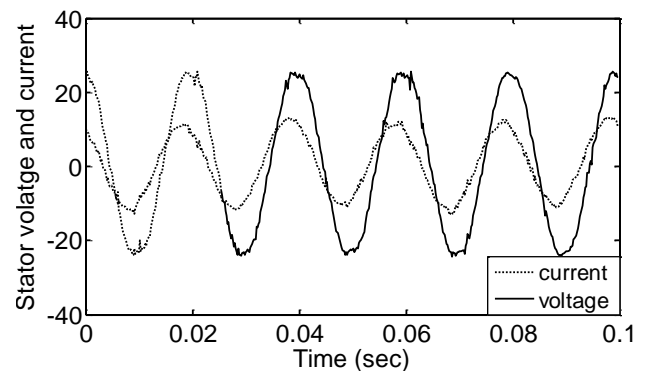


**Fig. 9.** *Waveforms of stator phase voltage and current of DFIM at ($I_2$=2.8A)*

### 5.  CONCLUSION

In this work, the performance of DFIG has been evaluated. Based on the experimental procedure, the generator characteristics are investigated under speed and load variation. The results demonstrate that the DFIG works as a synchronous generator. It possesses the power-angle characteristics and the V-curves of synchronous generator.

This paper presents the DFIG as a synchronous generator. This concept has been confirmed by experimental procedure. The machine characteristics are investigated under speed and load variation. The results demonstrate that the DFIM works as a synchronous motor. Its speed can be changed only by changing the rotor frequency and it is constant despite the load torque variation. It is not affected by the stator voltage or rotor voltage variation. Eventually, acceptable correlation between the theoretical and experimental results is achieved. This emphasizes the validity of the mathematical analysis.

# 6. REFERENCES

[1] Amin, Ifte Khairul, and M. Nasir Uddin. "MPPT based efficiently controlled DFIG for wind energy conversion system." 2017 IEEE International Electric Machines and Drives Conference (IEMDC). IEEE, 2017.

[2] Zheng, Xuemei, et al. "Full-order terminal sliding mode MPPT control for DFIG wind turbine system." 2017 12th IEEE Conference on Industrial Electronics and Applications (ICIEA). IEEE, 2017.

[3] Karakasis, Nektarios, et al. "Efficiency increase in a wind system with Doubly Fed Induction Generator." IECON 2016-42nd Annual Conference of the IEEE Industrial Electronics Society. IEEE, 2016.

[4] Jin, Shi, et al. "Constant V/Hz control based on DSP for open winding doubly-fed wind power generator." 2016 IEEE Transportation Electrification Conference and Expo, Asia-Pacific (ITEC Asia-Pacific). IEEE, 2016.

[5] Jiao, Lianwei, et al. "Doubly-fed induction generator (DFIG) as a hybrid of asynchronous and synchronous machines." Electric Power Systems Research 76.1-3 (2005): 33-37.

[6] Alkandari, Ahmad M., S. A. Soliman, and Mansour H. Abdel-Rahman. "Steady state analysis of a doubly fed induction generator." energy and power engineering 3.04 (2011): 393.

[7] Fan, Lingling, and Subbaraya Yuvarajan. "Modeling and slip control of a doubly fed induction wind turbine generator." 2008 40th North American Power Symposium. IEEE, 2008.

[8] Taoussi, Mohammed, et al. "Comparative study between Backstepping adaptive and Field-oriented control of the DFIG applied to wind turbines." 2017 International Conference on Advanced Technologies for Signal and Image Processing (ATSIP). IEEE, 2017.

[9] Wei, Chun, Wei Qiao, and Taesic Kim. "Low-voltage ride-through performance of sensorless vector controlled doubly-fed induction generators." 2017 IEEE International Conference on Electro Information Technology (EIT). IEEE, 2017.

[10] Li, Qing, et al. "Stator current vector control strategy of doubly fed induction generator using

proportional–resonant regulators." The Journal of Engineering 2017.13 (2017): 1728-1733.

[11] Marques, Gil D., and Matteo F. Iacchetti. "Sensorless frequency and voltage control in the stand-alone DFIG-DC system." IEEE Transactions on Industrial Electronics 64.3 (2016): 1949-1957.

[12] Elkhadiri, S., Elmenzhi, L., Lyhyaoui, A.: 'Fuzzy logic control of DFIG-based wind turbine'. Proc. Int. Conf. Intelligent Systems and Computer Vision, Fez, Morocco, April 2018, pp 1–5.

[13] Nazzal, Dham, and Abdel Latif Elshafei. "Performance improvement of a doubly-fed induction generator based WECS using intelligent techniques." 2017 Saudi Arabia Smart Grid (SASG). IEEE, 2017.

[14] Alalei, Abdelhakim, et al. "Adaptive sliding mode control of DFIG fed by matrix converter during grid faults." 2017 IEEE Conference on Energy Conversion (CENCON). IEEE, 2017.

[15] Pang, Songnan, et al. "Passivity full-order sliding mode control for DFIG wind turbine system." IECON 2017-43rd Annual Conference of the IEEE Industrial Electronics Society. IEEE, 2017.

[16] Xiahou, Kaishun, et al. "Robust rotor-current sensorless control of doubly fed induction generators." IEEE Transactions on Energy Conversion 33.2 (2018): 897-899.

[17] Chen, Minghui, et al. "Control strategy of excitation converter in Doubly-Fed Induction Generator wind power generation system." 2017 IEEE Conference on Energy Internet and Energy System Integration (EI2). IEEE, 2017.

[18] Zarei, Mohammad Ebrahim, Carlos Veganzones Nicolás, and Jaime Rodríguez Arribas. "Improved predictive direct power control of doubly fed induction generator during unbalanced grid voltage based on four vectors." IEEE Journal of Emerging and Selected Topics in Power Electronics 5.2 (2016): 695-707.

[19] Kadri, Ameni, et al. "Improved direct power control of a doubly fed induction generator based wind energy conversion system." 2018 5th International Conference on Control, Decision and Information Technologies (CoDIT). IEEE, 2018.

[20] Hazarika, Durlav, Ranjay Das, and Brajesh Gupta. "Improvement of bus voltage profile of a target bus using doubly fed induction generator-based distributed generator." 2017 International Conference on Power and Embedded Drive Control (ICPEDC). IEEE, 2017.

[21] Zhang, Debin, et al. "Dual-mode control for brushless doubly fed induction generation system based on control-winding-current orientation." IEEE Journal of Emerging and Selected Topics in Power Electronics 9.2 (2019): 1494-1506.

[22] de Santana, Marcelo Patrício, et al. "Vector control applied to mitigate the electromagnetic torque ripple in doubly fed induction generator." IEEE Transactions on Energy Conversion 36.4 (2021): 2977-2986.

[23] Soares, Emerson L., et al. "Dual Converter Connecting Open-End Doubly Fed Induction Generator to a DC-Microgrid." IEEE Transactions on Industry Applications 57.5 (2021): 5001-5012.

[24] Gao, Shuning, et al. "An improved direct power control for doubly fed induction generator." IEEE Transactions on Power Electronics 36.4 (2020): 4672-4685.

[25] Gayen, Pritam Kumar. "An Enhanced Rotor Position/Speed Estimation Technique for Doubly Fed Induction Generator Using Stator-Side Reactive Current Variable in Model Reference Adaptive System." IEEE Transactions on Industrial Electronics 69.5 (2021): 4409-4418.

**REVIEW:**

# INFLUENCE OF WAVE ENERGY CONVERTER TECHNIQUES AND MECHANISMS ON THE ENERGY PRODUCTION

## Ahmed S. Hassan[1*], Ali H. Alnajei[1], Mohammed Y[1]. Tharwan, Abdullateef H. Bashiri[1]

[1]Department of Mechanical Engineering, College of Engineering,Jazan University, P. O. Box 706, Jazan 45142, Kingdom of Saudi Arabia

**\*Corresponding author**

*Ahmed S. Hassan*

**Email address:**

*ashassan@jazanu.edu.sa*

Ocean and sea wave energy is one of the highest means of renewable energy sources. Methods of obtaining these energies must be progressing, since these resources are sustainable, unlimited, and environmentally friendly. In the present work, a comprehensive review of what researchers have presented in the field of techniques is done, also the mechanism for using these energies and how to convert these wave energies into electrical energy. Six different types of wave energy converters technology were evaluated, and the focus was on wave energy systems that produce electrical energy. It was concluded that although there have been many studies on wave energy technologies, there are still many energy converters devices that require improvements in the efficiency and reliability of these systems. Further research should be conducted to evaluate the effect of converter buoyancy shape on reliability and the coastal wall shape on the system efficiency. This research aims to achieve maximum energy recovery from wave energy inverters. Also, finding the best way to extract high energy and evaluate the applicable electrical devices through the appropriate selection of the control strategy. The problem of controlling the absorption of wave energy and torque of electrical machines and electronic power equipment is studied. The effect of control techniques on performance and power converters is conducted to help improve overall system performance when the wave converter is functional. It is found that the average power extraction increases in both regular and irregular waves by decreasing the power/torque of the power possessing.

*Keywords: wave energy converter; power point tracking; power take-up; oscillating water columns; buoys*

| Nomenclature: | | N | Wave action density spectrum, $m^2$/Hz |
|---|---|---|---|
| A | Area, $m^2$ | OWC | Oscillating Water Columns |
| a | Amplitude of the wave | PTO | Power Take-Off |
| c | Phase speed, ($=gT/2\pi$), m/s | P | Wave energy power or flux, kW/m |
| d | Sea water depth, m | S | Spectral density function, $m^2$/Hz |
| E | Wave energy spectrum density, W/Hz | T | Wave period, s |
| $F_b$ | Buoyancy force (N) | z | Displacement of buoys motion, m |
| | | $\sigma$ | Relative frequency, Hz |

| | | | | |
|---|---|---|---|---|
| $F_c$ | Current force (N) | | $\theta$ | Wave direction |
| $F_e$ | Excitation force (N) | | $\phi$ | Latitude, degrees |
| $F_f$ | Friction force (N) | | $\varphi$ | Velocity potential, $m^2$ /s |
| $F_r$ | Radiation force (N) | | $\rho$ | Density of sea water, $kg/m^3$ |
| $f$ | Wave frequency, Hz | | $\lambda$ | Wave length, m |
| $g$ | Acceleration of gravity, $m/s^2$ | | $\omega$ | Angular frequency, rad/s |
| $H$ | Wave height, m | | $\tau$ | Momentum of flux, $J/(m^2 s)$ |
| $h$ | Wave depth, m | | $\omega$ | Angular frequency rad/s |
| $k$ | Wave number, $(2\pi/\lambda)$, 1/m | | WEC | Wave Energy Converter |
| $m$ | Mass, kg | | | |

## 1. INTRODUCTION

Recently, due to the formation of the global warming phenomenon, attention has been paid to generating electric power from renewable energies. Ocean or sea wave energies are a type of renewable energy source that uses the power of waves to generate electricity. It differs from tidal energy, which uses the vertical movement of surface water that produces tidal waves. Simon [1] mentioned that wave energy is very promising in the future of renewable energies and has much energy when converted into electrical energy. Vivekraj [2] designed a Wave Energy converter (WEC) to generate electricity and to be a popular way to produce electricity in the future. Nevertheless, research in wave energy as a form of renewable energy is relatively low compared to other renewable energy technologies. Remote sensing provides effective platforms [3] for evaluating and mapping the temporal and spatiotemporal variability of ocean and sea wave energy on a global and regional scale. About 2000 TWh/year was obtained by exploiting wave energy [4, 5], which is about 10% of global electrical energy consumption. Also, they mentioned that wave energy has a higher density than solar energy and is more predictable and stable than wind energy. Elisabetta and Marta [6] showed that the control of the wave transducer gives a favorable trade-off for the high power extraction of applicable electrical devices. The use of more performance-rated power-taking (PTO) control techniques helps the initial PTO and improves the overall system performance. And the mean energy extraction is increased by computer simulations in both regular and irregular waves. Specific analyzes have to reduce the force/torque of the performance-rated power-taking.

In order to efficiently exploit the wave energy, a destructive interference must be created between the incident wave and the oscillatory motion of the primary WEC, and this requires effective device control. This requires a wave energy-absorbing machine with dynamic resistance and mechanical reactance that overcomes the opposing wave. Thus, to obtain the maximum power extracted from wave energy, the wave transducers, and actuator characteristics must be controlled. Various methods have been studied [6] to achieve maximum power and to a variety of optimization formulas. The power optimization control design of the WEC device [7, 8] have been studied through the use of a moment-based phase converter, which allows the application of the logarithms of the effective real-time. Polinder and Scuotto [9] recognized that the reason for the WECs slow development is that the ultimate goal of maximum power extraction is the whole system's economic feasibility. Ocean and sea wave energy have higher power than solar energy and are more stable than wind energy [10-12]. Several concepts of WEC have been studied, which focused on the mechanical structure, rate of energy conversion of different WECs [13-16]. To obtain the highest output power generated by a sea wave [7], the maximum output power in a point-type (MPPT) wave energy absorber is combined into a wave energy converter system.

The wave energy converter (WEC) is a device that converts received kinetic or frequency energy into electrical energy. The wave energy converter must be consisting of an efficient wave energy absorption, energy take-off technology, and produce smooth enough and has a high power electrical

energy. The main problem of wave energy devices is that they are not directly compatible with domestic traditional rotary electric machines. Due to the ease of fabrication and installation of the wave point absorber shown in Figure 1, which is a floating buoy to catch the wave and convert it into linear motion (WEC), it was considered the ideal solution for all wave energy conversion techniques [7, 17]. Besides, nowadays, there are many types of WECs available for point absorbers, including Ocean Power Technology's Power buoy [18] and Wavestar [19]. Given the current global warming conditions and the increasing energy demand, there is a need to find alternative ways to obtain clean energy and reduce future greenhouse gas emissions. The first method of generating continuous power from the waves is by using a floating body and taking advantage of its up and down movement through a gearbox with two generators, one working with the upward push of the wave and the other with the downward pull. This system consists of a floating buoy that captures wave energy and converts it into mechanical energy or up and down displacement. The float is connected simultaneously to a gear that converts vertical displacement into rotational motion according to the wave intensity. This gear is connected to the generator to be stored or used directly, and this system operates continuously in the same cycles.

The use of ocean and sea waves that carry very-large amounts of energy to generate electricity reduces global warming rates and reduces the demand for electricity produced from oil [20]. Farouk and others [21] mentioned that the wave energy is given energy of 550J/m2. The wave energy was estimated at more than 2 terabytes [22] and its use in generating electric power became common [23]. It was summarized [24] that the energy of the sea and ocean waves is given (2-3 kilowatt hours/square meter), while wind energy is given (0.4 - 0.6 kilowatt/square meter) and solar energy (0.1-0.2 kilowatt-hour / square meter). However, the use of these energies requires converting the movement of reciprocating waves up and down into rotational movement and then converting it into electrical energy [25, 26]. Four different wave energy converter absorption control methods have been proposed to improve wave energy capture: (a) phase and amplitude control [27-29], (b) complex coupled control [30-33], (c) predictive model control (MPC) [34-38], and (d) maximum control [39-43]. Phase and amplitude control of a

finite amplitude floating wave converter are described [19], whereby phase control is applied to maintain the buoyancy velocity with the wave's excitation power and this gives a result similar to lock-up. This method is effective in maximizing energy extraction from an absorption point. The body's ability to absorb wave energy depends on its hydrodynamic design. The main objective of wave transducer control (WEC) is to use power takeoff (PTO) to change the amplitude or phase of the motion to bring it close to the optimum state. Wave transducers can be classified into four types: oscillating water columns (OWCs), attenuators, bypass, and point absorbers. Manhar et al. [44] give the hydrodynamic dimension of some WEC techniques for average wave conditions and capture ratio. They mentioned that the length of the floating superstructure device (12-20 m) at 17% capture rate, the oscillating water column with the thickest dimension and 29% capture rate, the absorption point diameter (12-20 m) with 16% capture rate, and the slope longer than a wavelength (Fixed bottom) at 37% capture rate. The oscillating water columns are the most well-known and widely used, and these devices are fixed either onshore or nearshore and classified into two types floating and immovable [45].

## 2. THEORY AND APPLICATIONS OF WAVE ENERGY CONVERTERS

Wave Energy Converters (WECs) depend in their design on many parameters such as the mode of wave motion, electrical generation systems, and their location from shore. The mechanism converted the sensed wave energy by the WEC into power on the wire is the power take-off system (PTO). At the PTO output, a practical power form is available. WEC can be Oscillating Water Columns (OWC), surface attenuator, or any convenient converter type. External power take-off mechanisms are based on high-pressure hydraulic systems, wind turbines, and linear generators. The PTO system consists of a sea wave transducer (WEC), compressor, tank, turbine, and generator. Because the float device always takes the same movement of the surface of the water, the difference between the maximum and minimum values in the height of the wave used leads to the activation of the generator directly connected to the floating body. The improved method for the PTO is

presented in Farrok, et. al., [46]. The most used method of electricity production is made after the conventional high-speed rotary electrical generators [47]. Where the performance of a converter is measured efficiently as the energy conversion between wave energy and electrical energy generated or by the load factor, which is equal to the electrical energy produced on the wire divided by the rating of the input wave energy at the system input [48]. The monochromatic wave method is one of the most widely used methods for analyzing the random behavior of sea and ocean waves. This method is based on a single transient wave of sinusoidal shape is most commonly used to analyze the behavior of sea and ocean waves. To analyze the energy of the sinusoidal wave, a simple harmonic function (regular wave) in the x-axis direction is produced (Fig. 1) as:

$$Z(t, x) = 0.5h_w \sin(\omega t - kx) = 0.5h_w \sin[(2\pi t/T) - (\pi x/\lambda)] \quad (1)$$

Where $h_w$ is the significant high of the wave, $\lambda$ is the wave length, T is the period, $h_{depth}$ is the water depth, g is the gravity acceleration of, and k is the wave number. Substitute the wave velocity ($C = \lambda/T_w$) into equation (1) and rephrase it as follows:
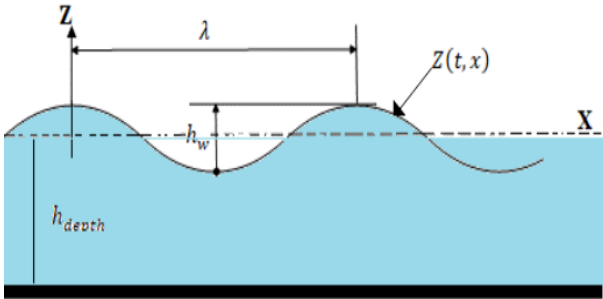


**Fig. 1.** Significant parameters of the regular wave depth

$$Z(t, x) = 0.5h_w \sin[(2\pi/\lambda)(Ct - x)] \quad (2)$$

Although waves near the shore produce less energy, they are characterized by the simplicity of installing and maintaining transducers. The wave energy flux ($P_{wave}$) based on the average wave energy density per unit horizontal area can be found as:

$$P_{wave} = 0.625\rho gh^2_w (gh_{depth})^{0.25} \quad (3)$$

Using definition of the velocity in deep, ($C_g = (gh_{depth})^{0.5}$, shallow water is considered when $h_{depth} \leq \lambda/2$, whereas deep water is for $h_{depth} \geq \lambda/2$, the wave average power (kW), using Equ.(3) becomes:

$$P_{wave} = 0.689h^2_w T_w \quad (4)$$

## 3. WAVE ENERGY TECHNOLOGY

Wave devices are classified by the location of their propagation (onshore, nearshore, offshore), the method of capturing wave energy, and energy take-off systems. Implemented systems can be fixed, submerged, or floating. The systems can be used as standalone generators or as part of breakwaters or port infrastructure. Wave energy transmission techniques were classified as follows: the first type is the Point Absorption Buoy (PAB) which consisting of a cylinder fixed vertically in the water and is either floating or submerged and depends on the pressure difference [49]. Sea wave drives the PAB system vertical movement of the buoy connected to a linear piston-based generator to produce continuous power [50]. The generator is installed on an underwater piling, and the power is transmitted to the shore via cables. The advantages of the PAB system are no dependence on wave direction, simple design, manufacture, installation, and maintenance, low cost. The second type is the surface attenuator which is a mechanical structure operating at an offshore site with multiple floating objects connected by couplings. Hinged joints contain hydraulic cylinder piston arrangements driven by a motor connected to a generator. The third type is the oscillating wave impulse converter consists of a hinged, submerged reflector that moves forward and backward, positioned perpendicular to the direction of the wave [51], so that this movement is transmitted in a piston-based system to produce energy. The fourth type [52] is the oscillating water column (OWC) which consists of an air chamber and a power take-off (PTO) system so the air chamber opens on the seashore to receive the wave energy and convert this energy into compressed air that passes through the turbine in the external power intake mechanism. The fifth type is the bypass device [53], which captures the incident wave energy by a water storage tank above sea level and releases the water back into the sea through a hydro turbine, similar to a hydroelectric power station. This device has high efficiency compared to other wave transducers.

## 4. MODELING ANALYSIS OF THE POINT-ABSORBING TYPE OF THE WEC AND POWER SPECTRUM

The effects of wave period on wave energy absorption efficiency of buoys and hydraulic systems can be analyzed using the energy equation. Figure 2 shows an analysis of the forces acting on the buoy, which are the gravitational force mg, the buoyant force $F_f$, the wave force $F_V$, the hydrostatic recovery force $F_S$, and the hydraulic damping force f, so that the forces of gravity and buoyancy are equal in magnitude and opposite in direction. Based on the energy equation principle, the equivalent damping force $F_C$ along the z-axis has the same working effect for the float as the hydraulic damping force F. The floats produce minor harmonic vibrations affected by these forces in the vertical direction, where the equivalent damping force $F_C$ is in the opposite direction of wave force, $F_V$. The force is analyzed according to the Newton's second law and written as:

$$F_C + F_S + F_V = (m+m_w)\ddot{y} \tag{5}$$

Where m is the buoy mass of a horizontal cylinder, $m_w$ is the buoy added mass ($m_w = \pi\rho R^2 L/2$), R and L are the cylinder radius and length. The buoys wave force, $F_V = F_o \cos\omega t$, where $F_o$ is the wave force amplitude, $\omega$ is wave frequency. The equivalent damping force, $F_C = (-8CR^2/L^2)(1-r)\dot{y}$, where, $\dot{y}$, $\ddot{y}$ are the heaving motion speed and acceleration. The hydrostatic restoring force is $F_S = \rho g Y A_W$, where, $A_{WP}$ is the buoy wetted surface, $A_{WP} = 2L(2dR-d^2)^{0.5}$, d is the buoys immersed depth, and, C is the damping coefficient, ($C=V_c/f$), where, $V_c$ is the speed of the hydraulic cylinder piston, r is introduced as the proportionality coefficient of speed ($r = \dot{y}_o/\dot{y}$), y is the displacement of buoys heaving motion. Using the above definitions, Equ. (1), becomes:

$$F_o \cos\omega t = (m+m_w)\ddot{y} + (-8C\,R^2/L^2)(1-r)\ddot{y} + rgYA_{WP} \tag{6}$$

The buoy wave absorption power, $P_c$ can be written as:

$$P_C = (C/T)\frac{C}{T}\int_0^T [2(1-r)Ry)/L]^2 \, dy \tag{7}$$

, and the hydraulic system wave absorption power is:

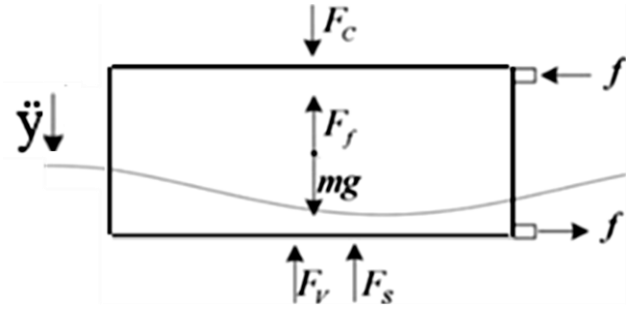$$P_F = \frac{1}{T}\int_0^T F_V \, y\,dt \tag{8}$$



**Fig. 2.** Analysis of the forces acting on the buoy

The efficiency of the wave energy conversion can be written as Ruellan et al. [48] and using Equs. (5 – 8) as:

$$\eta_c = P_C/P_{Sea}, \text{ and } \eta_f = P_F/P_{Sea} \tag{9}$$

Where, $\eta_C$ and $\eta_F$ are the wave energy absorption efficiency of buoys and hydraulic system respectively, $P_C$, and $P_F$ are the average wave energy absorption power of buoys and hydraulic systems, $P_{Sea}$ is the input power of the wave, ($P_{Sea}=\rho g^2 GTH^2/32$), G is the immersed width of buoys. Where electrical and power electronics transformers make up the electrical power system. One of the wave energy conversion systems consists of a spherical absorber with a semi-submerged point in one case arranged in a vertical motion by sea waves. This vertical motion is transmitted to a rotating electric generator driven by a pneumatic power interface, with no hydro or intermediate phase. The mechanical gearbox is only used to convert the linear motion into a rotating gearbox and to adapt the slow speed of the float movement to the speed of the mechanical machines, based on the solution presented in [6]. The mean average power ($P_{wavg}$) in the steady-state waveform is given by the mean value of the sine power waveform as a function of the load power factor, angular frequency $= 2\omega$, and corresponding to the energy dispersed over the load impedance RL, is:

$$P_{wavg} = (E^2 R_L)/[(R + R_L)^2 + \left([\omega L - (\frac{1}{\omega C}) \pm R_L(1 - \cos^2\varphi_L\right)^{0.5}/\cos\varphi_L^{\,2}] \tag{10}$$

In the case of the wave amplitude (A) = 0.5m, wave period, T = 9 s, buoy mass, M=268340kg, added mass, a=202700kg, buoy radius, R=5m, spring

stiffness, K=789740N/m, and total buoy damping, B= 57400kg/s. The maximum instantaneous power transferred to the load can be obtained when $[\pi - \varphi_L =2(wt+bL)]$ and is expressed as a function of the load resistance and power factor which is:

$$P_{max} = P_{wavg} \left(1 + 1/cos\varphi_L\right) \quad (11)$$

To estimate the variation in the absorption power, average power, and the incoming wave power with the wave period with the buoy, hydraulic systems, and efficiency of the absorption Equs. (7-11) are used and represented in figures 3, and 4. Figure 3 shows the effects of the wave amplitude on the efficiency of the absorption. It is clear from the results represented in this figure that the highest absorption efficiency of the system is at a wave amplitude of about 1.5 with an efficiency of up to 98% and decreases with the increase or decrease of this wave amplitude. Also, the results of the present theoretical analyses and the theoretical results of [6] are shown in the figure and show good agreements. The average and peak power for these conditions can be represented by taking into account the effect of wave amplitude changes on the average and peak power absorption in Fig. 4. The figure shows increase of the all of the maximum and average powers by increasing the wave amplitude. It can be concluded that this design, along with the assumptions made, affected the peak power and average power extraction, making this type of wave converter the favorable one. On the other hand, to study the effects of different incident sine waves on the ability performance of the point absorber and to control it so as not to exceed the maximum power. It is useful to analyze the difference in applying the tuned control strategy to conventional passive loading and complex conjugated control using fixed parameters. Doing so requires that the sinusoidal incident waves have a constant period of about T = 9s and that the negative loading and complex control factors remain constant at their optimum value corresponding to the sinusoidal conditions. An example of the above described was applied by Ozdamar et al. [49] to a wave energy system consisting of an oscillating water column, a baffle (front wall), a wave turbine, an electric generator, and an air chamber (an air column).
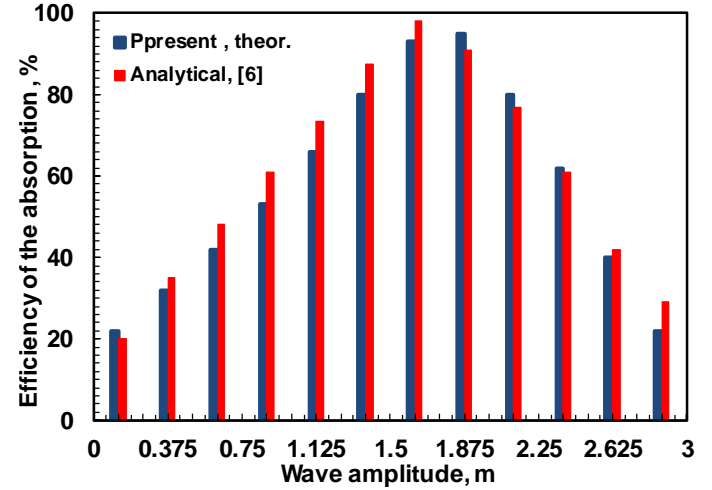


**Fig.3.** Present and analytical results of [6] for the efficiency of the absorption
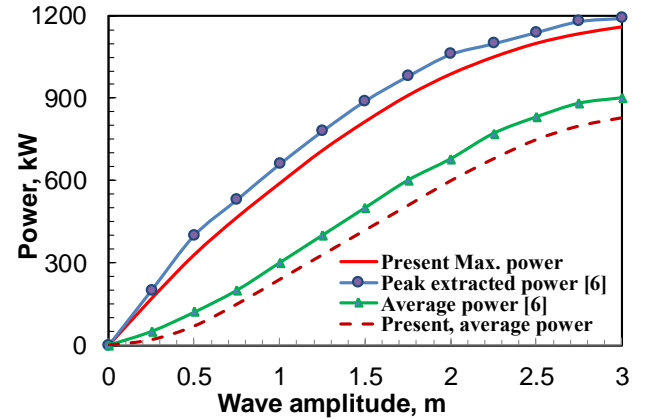


**Fig. 4.** Peak and average power of the present analyses and Elisabetta et al. [6]

Ozdamar et al. [49] assumed that the flow was unstable and incompressible and changed the dimensions of the air chamber to change the wave parameter to increase the efficiency of the system. The efficiency of the oscillating water column system increased to 67% and then decreased to 50% as the wave amplitude increased. In this research, the Ansys program was used on this system to make a comparison with the published results of [49] to find out the wavelength of the wave on the efficiency of this type of absorber and transmitter as shown in Figure 5. This was implemented for the wave transducer by dividing the power of water flow ($P_{flow} = 0.5\rho_a AV^3$) over the wave force ($P_{wave} = \rho g^2 H^2 TC[1+2kd/sin(2kd)]/(64\pi)$. Where d is the water depth, and A is the cross-sectional area of the

chamber along the direction of current-wise, C is the horizontal wave velocity, and V is the air speed in the vertical air chamber. The present results are compared with the results obtained by the researcher [49], which indicates an acceptable convergence between them using the Ansys program. The figure shows the highest efficiency is reached at a wave amplitude of 6 cm, and this efficiency decreases with the increase and decrease of the mode value from this figure. It is clear from the figure that this type of wave picker and its conversion into mechanical energy works at a small wavelength in conjunction with other devices mentioned earlier in this research. The wave transmission efficiency is lower than the previous one, as in Figure 5, where the wave transmission efficiency reached 97% at wavelength 1.5-1.8, while the highest efficiency in this type reached about 72%. The figure shows the highest efficiency occurs at a wave amplitude of 6 cm, and this efficiency decreases with the increase and decrease of the mode value from this figure. It is clear from the figure that this type of wave picker and its conversion into mechanical energy works at a small wavelength in conjunction with other devices mentioned earlier in this research. The wave transmission efficiency is lower than the previous one, as in Figure 5, where the wave transmission efficiency reached 97% at wavelength 1.5-1.8, while the highest efficiency in this type reached about 72%. That means that the direct coupling point absorption in the heave system gives good efficiency than the oscillating water column system.
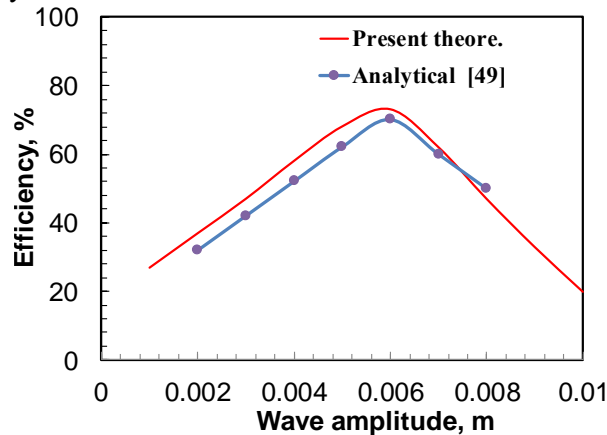


**Fig. 5.** Efficiency vs wave amplitude of OWC, present analyses and [49]

## 5. EFFECT OF BUOY DESIGN PARAMETERS

Several studies have been conducted on the concepts of wave energy converters (WECs), while the present work study effects of the mechanical structure, hydrodynamic aspect, and energy conversion rate on the WECs wave energy conversion methods. A point absorber device, which was considered the promising solution in wave energy conversion techniques due to the ease of manufacturing and installation. Where the wave energy is captured by floating floats in this device and converted into linear motions. And there are several types of point absorption-type WECs is available including the ocean power technology's power buoy [18] and Wavestar [19]. However, its frequency response was narrow, which reduced its performance in irregular wave conditions. To improve the wave energy capture, and improve the absorption point efficiency, the wave energy generation system must capture the maximum energy for the real sea conditions. It is well known that the waves of seas and oceans are multiple and irregular through varying frequencies and amplitudes. To describe these waves analytically an energy spectrum was generated by Bretschneider that has been widely adopted based on representative sea state parameters. However, the spectrum that depends on the significant wave height H and the spectrum peak period $T_p$, is:

$$S(\omega) = 5H^2(\pi^4/T_p\omega^5)e^{1.25(2\pi/\omega Tp)4} \qquad (12)$$

The irregular excitation time-domain that can be obtained from the energy spectrum of $1.25(2\pi/\omega T_p)^4$, and the wave amplitude is $A_i(\omega_i) = [2S(\omega_i)\Delta\omega]^{0.5}$. Where $\Delta\omega$ is the wave spectrum discretization and $\varphi_i$ is the random phase angles from 0 rad to $2\pi$ rad. Accordingly, the excitation force coefficient $f_{exc}(t)$ can be written as:

$$F_{exc}(t) = \sum_{i=1}^{N} A_i f_{exc}(\omega_i)\cos(\omega_i t + \varphi_i) \qquad (13)$$

Figure 6 shows the energy spectrum obtained using Equs 12 and 13 through the selected wave period and the height of the great sea wave. The figure indicates that the available wave energy range is from 0.35 rad/s to 1.15 rads/s and the maximum at about 0.6 rads/s, while the wave energy density of other frequencies is very small and can be ignored when the

power control is performed in the wave power generation system. Figure 7 shows an example of an excitation strength curve with a large wave height (H =1.7m) and peak period of the spectrum (Tp=8s). The Power oscillating water columns ($P_{OWC}$) absorbed from the waves by an oscillating water columns device depends on the total pressure, the velocity of the air, and the area is:

$$P_{owc} = 0.25\pi V D^2 \ (P_s+0.5\rho_a V^2) \qquad (14)$$

Where $P_s$, is the air static pressure, V is the air velocity, and D is the duct diameter. The power of incident water wave ($P_W$) across the width of an Oscillating Water Columns (OWC) device is given by [41]:

$$P_w = \rho_w g^2 H^2 T b/32 \qquad (15)$$

where $\rho_w$, g, H, T, and b is the water density, the gravity acceleration, the wave height, the wave period and the width of the OWC respectively.
The efficiency of the oscillating water columns is a measure of how much power is extracted by the device from the incoming wave. Therefore, the efficiency of the OWC system, from Equs. (14, and 15) is given by:

$$\eta_{owc}=P_{owc}/P_w=8\pi V D^2(P_s+0.5\rho_a v^2)/(\rho_w g^2 H^2 Tb) \quad (16)$$

here $P_s$ is the average total pressure, and $0.5\rho_a v^2$ is the average air velocity. Figure 8 shows the spectrum of the energy produced from using the power oscillating water column system of the current analyses using the ANSES program, and the results gained by [7]. The figure shows the accepted agreements for the results. It is also evident in the figure that at frequency 7 Hz, the generated power is the maximum value and decreases after and before this frequency, and the remaining energy at the low frequency is ignored due to its small values.
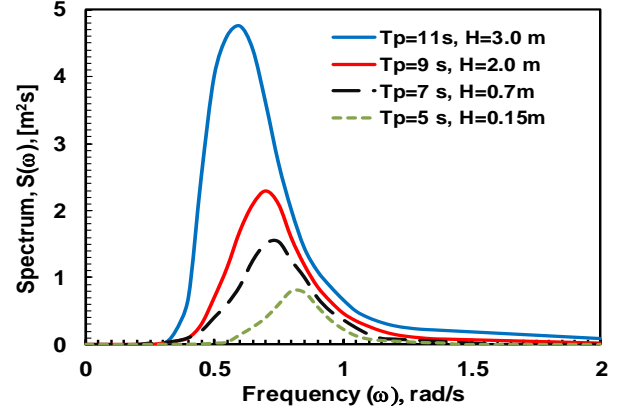


**Fig. 6.** Wave energy spectrum according to Bretschneider model
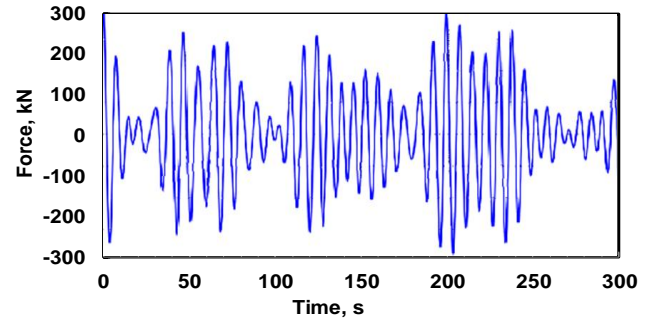


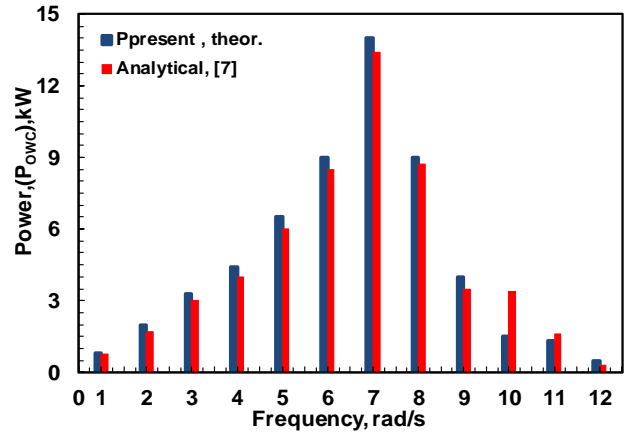**Fig. 7.** Time-domain excitation force for irregular waves



**Fig. 8.** Power oscillating water columns ($P_{OWC}$), present, [7]

## 6.   CONTROL OF POINT ABSORBERS

From previous reviews, it was found that WEC has a specific uptake period of the control point. It occurred when the period of the incident wave coincided with the period of WEC. It is therefore recommended to

adjust the natural resonant frequency of the WEC according to the frequency of the incoming wave. Thus, the WEC can be controlled using force take-off (PTO) to change the amplitude and bring it closer to the optimum state. From here both the amplitude and phase of the WEC motion are controlled so that the resonant state of the PTO can be achieved by applying one component proportional to the speed of the WEC and another proportional to the acceleration of WEC. The effect of wave period on the wave energy absorption efficiency of buoys where the damping coefficient of the hydraulic system is shown in Figure 9. The wave energy absorption efficiency of buoys reaches its maximum of 65% when the wave period is in the range of 3.0 s to 3.5 s, and outside this range, it decreases rapidly. The natural frequency of floats is also in the range. When the wave period is 2.5 seconds, its efficiency can be reduced to less than 10%.
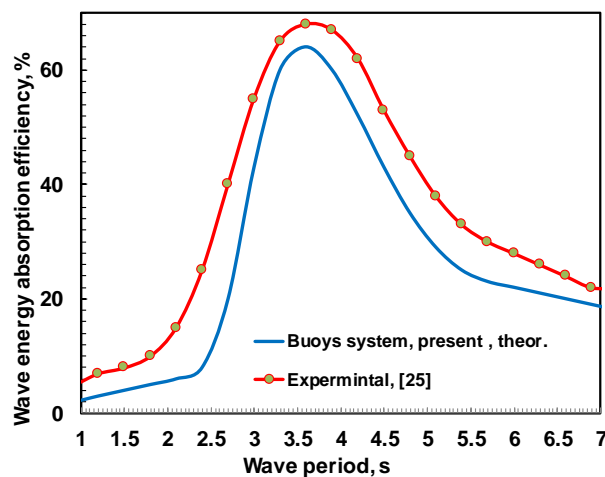


**Fig. 9.** Variation of wave energy absorption efficiency with wave period

## 7.  CONCLUSIONS

Due to the global warming conditions and the increase in pollution rates, the world is turning recently to use different types of renewable energies, such as solar, wind, and wave. It is clear from examining many published works in the field of utilizing sea and ocean wave energy, the consensus was noted that sea and ocean waves have much higher energy than the energy of the wind and solar. Wave energy is given the highest amount for other different renewable energies, as it gives 2-3 kW/m$^2$ compared to the wind which gives 0.4-0.6 kW/m$^2$, and solar

energy gives 0.1-0.2 kW/m$^2$. In other words, the cost of generating electrical energy from wave energy is higher than the cost of generating traditional fossil fuels, solar energy, or wind energy. Therefore, wave energy is the least used in generating electrical energy. Because of the power transmission problems or carrier efficiency due to poor wave transducer technology.

Examining many previously published papers concludes that most wave energy converter systems (WECs) are similar and have low efficiency. This research focused on the principles of wave energy that stand behind the development of energy production from sea or ocean waves, methods of converting it into electrical energy, and the efficiency of wave transmission. Also, the present work investigates the current technologies based on the operational and technical characteristics of wave power inverters, their applicability, and future growth in this sector. This research focused on finding the best ways to transfer wave energy and the best devices that give the highest efficiency for converting wave energy into electric energy.

## 8.   REFERENCES

[1]  Neill, Simon P. "Introduction to Ocean Renewable Energy." *Reference Module in Earth Systems and Environmental Sciences, Elsevier* (2021).

[2]  Vivekraj, M., "*Design and Development of Ocean Wave Energy Power Generation System*", Int. J. of Eng. Res.& Tech. (IJERT), Published by: www.ijert.org Vol. 10, Issue 03, March 2021. 91-92.

[3]  Seenipandi, Kaliraj, K. K. Ramachandran, and Pavan Kumar. "Ocean remote sensing for spatiotemporal variability of wave energy density and littoral current velocity in the Southern Indian offshore." *Remote Sensing of Ocean and Coastal Environments*. Elsevier, 2021. 47-63.

[4]  Robertson, B., "Wave Energy: Resources and Technologies", Reference Module in Earth Systems and Environmental Sciences, 2021.

[5]  Brekken, Ted KA, Annette Von Jouanne, and Hai Yue Han. "Ocean wave energy overview and research at Oregon State University." *2009 IEEE Power Electronics and Machines in Wind Applications*. IEEE, 2009.

[6] Tedeschi, Elisabetta, and Marta Molinas. "Tunable control strategy for wave energy converters with limited power takeoff rating." *IEEE Transactions on industrial electronics* 59.10 (2011): 3838-3846.

[7] Zhao, Aqiang, et al. "A flower pollination method based global maximum power point tracking strategy for point-absorbing type wave energy converters." *Energies* 12.7 (2019): 1343.

[8] Faedo, Nicolás, et al. "Energy-maximising control of wave energy converters using a moment-domain representation." *Control Engineering Practice* 81 (2018): 85-96.

[9] Polinder, Henk, and Mattia Scuotto. "Wave energy converters and their impact on power systems." *2005 International conference on future power systems*. IEEE, 2005.

[10] Uihlein, Andreas, and Davide Magagna. "Wave and tidal current energy–A review of the current state of research beyond technology." *Renewable and Sustainable Energy Reviews* 58 (2016): 1070-1081.

[11] Alkhayyat, Misaa, et al. "Wave energy converters: Barriers and drivers." (2020).

[12] Al Yousif, Mohammed Ahmed, and Al Yousif. "Renewable Energy Challenges and Opportunities in the Kingdom of Saudi Arabia." *International Journal of Economics and Finance* 12.9 (2020): 1.

[13] Ozkop, Emre, and Ismail H. Altas. "Control, power and electrical components in wave energy conversion systems: A review of the technologies." *Renewable and Sustainable Energy Reviews* 67 (2017): 106-115.

[14] Gaspar, José F., et al. "Design tradeoffs of an oil-hydraulic power take-off for wave energy converters." *Renewable energy* 129 (2018): 245-259.

[15] Wen, Yadong, et al. "A shape optimization method of a specified point absorber wave energy converter for the South China Sea." *Energies* 11.10 (2018): 2645.

[16] Kolios, Athanasios, et al. "Reliability assessment of point-absorber wave energy converters." *Ocean Engineering* 163 (2018): 40-50.

[17] Meng, Fantai, et al. "Modal analysis of a submerged spherical point absorber with asymmetric mass distribution." *Renewable Energy* 130 (2019): 223-237.

[18] OPT- Ocean Power Technology, Available: http://oceanpowertechnologies.com/accessed on 20 Dec. 2018.

[19] Wavestar, Available online: http://wavestarenergy.com, accessed on 20 Dec. 2018.

[20] Farrok, Omar, et al. "Electrical power generation from the oceanic wave for sustainable advancement in renewable energy technologies." *Sustainability* 12.6 (2020): 2178.

[21] Farrok, O., Islam, M., and Sheikh, M., "Analysis of the Oceanic Wave Dynamics for Generation of Electrical Energy Using a Linear Generator," J. of Energy 2016 (2016): 1-14.

[22] Amir, Mohamad Abu Ubaidah, et al. "Wave energy convertors (WEC): A review of the technology and power generation." *AIP Conference Proceedings*. Vol. 1775. No. 1. AIP Publishing LLC, 2016.

[23] Drew, B., Plummer, R., and Sahinkaya, N., "A Review of Wave Energy Converter Technology", J. of power energy, Proc. IMechE, Vol. 223, Part A, pp. 887-902, 2009.

[24] Huang, Lei, et al. "Winding configuration and performance investigations of a tubular superconducting flux-switching linear generator." *IEEE Transactions on Applied Superconductivity* 25.3 (2014): 1-5.

[25] Gao, Hongtao, and Biao Li. "Establishment of motion model for wave capture buoy and research on hydrodynamic performance of floating-type wave energy converter." *Polish Maritime Research* 22.S1 (86) (2015): 106-111.

[26] Zhen, L., Cui Y., Zhao H., Shi H., and Hyun S. "Effects of damping plate and taut line system on mooring stability of small wave energy converter." *Mathematical Problems in Engineering* 2015 (2015).

[27] Waters, Rafael. *Energy from ocean waves: full scale experimental verification of a wave energy converter*. Diss. Universitetsbiblioteket, 2008.

[28] Chenari, B., Saadatian, S., and Ferreira, A., "Wave Energy Systems: An Overview of Different Wave Energy Converters and Recommendation for Future Improvements", 8th International Technology, Education and Development Conf., Valencia, Italy, pp.10-12, 2014.

[29] Dizadji, Nader, and Seyed Ehsan Sajadian. "Modeling and optimization of the chamber of OWC system." *Energy* 36.5 (2011): 2360-2366.

[30] Park, Joon Sung, et al. "Active phase control for maximum power point tracking of a linear wave generator." *IEEE transactions on power electronics* 32.10 (2016): 7651-7662.

[31] Têtu, Amélie, et al. "Physical and mathematical modeling of a wave energy converter equipped with a negative spring mechanism for phase control." *Energies* 11.9 (2018): 2362.

[32] Liu, Changhai, Qingjun Yang, and Gang Bao. "Latching control using optimal control method for a raft-type wave energy converter." *Ships and Offshore Structures* 13.sup1 (2018): 138-154.

[33] Temiz, Irina, et al. "Economic aspects of latching control for a wave energy converter with a direct drive linear generator power take-off." *Renewable energy* 128 (2018): 57-67.

[34] Cantarellas, Antoni Mir, Daniel Remon, and Pedro Rodriguez. "Adaptive vector control of wave energy converters." *IEEE Transactions on Industry Applications* 53.3 (2017): 2382-2391.

[35] Song, J., Abdelkhalik, O., Robinett, R., Bacelli, G., Wilson, D., and Korde, U., "Multi-resonant feedback control of heave wave energy converters." *Ocean Engineering* 127 (2016): 269-278..

[36] Abdelkhalik, O., Zou, S., Robinett, D., Bacelli, G., Wilson, G., Coe, R., Korde, U "Multiresonant feedback control of a three-degree-of-freedom wave energy converter." *IEEE Transactions on Sustainable Energy* 8.4 (2017): 1518-1527.

[37] Anderlini, E., Forehand, I., Stansell, P., Xiao, Q., and Abusara, M. "Control of a point absorber using reinforcement learning." *IEEE Transactions on Sustainable Energy* 7.4 (2016): 1681-1690.

[38] Anderlini, E., Forehand, I., Bannon, E., Abusara, M., "Control of a realistic wave energy converter model using least-squares policy iteration." *IEEE Transactions on Sustainable Energy* 8.4 (2017): 1618-1628.

[39] Xu, L., Li, Y., Lin, L. "An Improved Boundary Element Method for Modelling a Self-Reacting Point Absorber Wave Energy Converter", Acta Mech. Sin. 34 (2018): 1015 -1034,.

[40] Xiao, X., Huang, X., Kang, Q., "A Hill-Climbing-Method-Based Maximum-Power-Point-Tracking Strategy for Direct-Drive Wave Energy Converters", IEEE Trans. Ind. Electron., 63 (2016): 257 - 267.

[41] Mahnamfar, F., and Altunkaynak, A., "Comparison of Numerical and Experimental Analyses for Optimizing the Geometry of OWC Systems". Ocean Engineering, Elsevier, 130 (2017) 10-24.

[42] Lendenmann, H., Stromsem, C., Daipre, M., Arshad, W., Leirbukt, A, Tjensvoll, G., and Gulli, T., "Direct Generation Wave Energy Converters for Optimized Electrical Power Production," in Proc. 7th EWTEC, Porto, Portugal, September 11–13 (2007) 1–10.

[43] Rahman, Abidur, et al. "Recent progress in electrical generators for oceanic wave energy conversion." *IEEE Access* 8 (2020): 138595-138615.

[44] Pecher, Arthur, and Jens Peter Kofoed. *Handbook of ocean wave energy*. Springer Nature, 2017.

[45] Ruellan, M., Ben Ahmed, H., and Multon, B., "Design methodology for a SEAREV wave energy converter." *IEEE Transactions on Energy Conversion* 25.3 (2010): 760-767.

[46] Farrok, O., Islam, R., Sheikh I., Guo, Y., Zhu, J., and Lei, G., "Oceanic Wave Energy Conversion by a Novel Permanent Magnet Linear Generator Capable of Preventing Demagnetization", IEEE Transactions on Industry Applications, 54(6) (2018) 6005-6014.

[47] Prendergast, J., Li, M., and Sheng, W., "A Study on the Effects of Wave Spectra on Wave Energy Conversions", IEEE Journal of Oceanic Engineering, (2018) 1-13.

[48] Nanjundan, P., Kui, M., Yoon, H., and Yeon, Y, "Ocean Wave Energy Converters-A Perspective." *Journal of Advanced Marine Engineering and Technology* 36.5 (2012): 707-715.

[49] Ozdamar, G., Y. Pekbey, and A. Ozdamar. "A Numerical Study of the Effect of Wave Amplitude on the Efficiency of a Wave Power System." *Acta Physica Polonica, A.* 134.1 (2018).

[50] Kempener, R., and Neumann, F., "Wave energy technology brief, IRENA Ocean Energy Technology Brief", www.irena.org, 2014.

[51] Rahman, Abdullah Al Mahfazur, Md Moniruzzaman, and M. Al Mamun. "Estimation of energy potential of point absorber buoy type

wave energy converter." *2017 3rd International Conference on Electrical Information and Communication Technology (EICT).* IEEE, 2017.

[52] Jebli, M., and Chagdali, M., "Hydrodynamic Characteristics of OWC Device for Wave Energy Conversion", Renewable Energies, Power Systems & Green Inclusive Economy, Casablanca, Morocco, (2018) 1-5.

[53] Houhou, R., Do S., Kha, S., and Azee A., "Feasibility Study on Converting Ocean Waves Energy by Pelamis in United Arab Emirates", Int. Conf. (ASET), Abu Dhabi, UAE (2018) 1-5.

# AN ANALYTICAL EXPLORATION AND MATHEMATICAL MODELING ON THE DYNAMICS OF SEA WAVE ENERGY CONVERSION TO ELECTRICITY PRODUCTION

*Ahmed S. Hassan [1*], Mohammed Y. Tharwan[1], Yahya A. Rothan[1], Haitham M Hadidi[1]*

[1]Department of Mechanical Engineering, College of Engineering, Jazan University, P. O. Box 706, Jazan 45142, Kingdom of Saudi Arabia

**\*Corresponding author**

*Ahmed S. Hassan*

**Email address:**

*ashassan@jazanu.edu.sa*

Recently, most countries suffering from global warming due to the waste gases coming out of the combustion engines used to generate electric power by traditional methods. Therefore, many countries are currently trying to find alternative solutions to this problem by using renewable energies such as solar energy, wind energy, and energy generated from the waves of the ocean and sea to overcome pollution problems. The waves of the seas and oceans have enormous and largely untapped energy, so this work presents an efficient way to use the energy of sea waves to generate electricity. And also, trying to be a way to produce electricity from wave energy in the future. The best suitable places along the shores of Jizan city were inspected to install the buoy system to revenue advantage of the wave supreme height to achieve the height amount of electrical energy. A mathematical model was made to analyze the wave energy and convert it into energy extracted by mechanical force. The mathematical analyzes used the data collected from satellite maps of the numerous severe waves in the Red sea of the Jazan area, and the data published in previous research along that area. It was found that the beach of the Al Shuqaiq area is the greatest for installing the buoy and obtaining the highest electrical energy due to the presence of the highest wave intensity, followed by the beach of the Baysh and Al Morgan area.

Also, one of the objectives of this research is to study the design of a device powered by a buoy to use the waves of the Red Sea to generate electric power. The influence of the buoy system design parameters such as the buoy diameter, length of the cylinder, and the length of the connecting rod on the electrical energy generation from wave energy was investigated. The current device is designed with a gearbox to produce continuous power with a single electric generator. A floating mooring device uses the rise and fall of bulges to convert sea wave energy into electrical energy. The device consists of a float, arm, two wheels of different diameters, a gear set, and an electric generator. The effect of the design of several factors on the performance of the device for converting the sea waves energy into electrical energy, including the length of the buoy arm, the wave height by changing the cam diameter, and the conversion ratios between the gear set, to optimize the output power of the wave energy.

*Keywords:* Wave, Energy; Dynamics, Modeling; Generator; Converter, linear

**Nomenclature:**

| | | | |
|---|---|---|---|
| A | Area, $m^2$ | P | Wave energy power or flux, kW/m |
| a | Amplitude of the wave | S | Spectral density function, $m^2$/Hz |
| c | Phase speed, $(=gT/2\pi)$, m/s | S | Net input energy, kW |
| d | Sea water depth, m | T | Wave period, s |
| E | Wave energy spectrum density, W/Hz | z | Displacement of buoys motion, m |
| f | Wave frequency, Hz | σ | Relative frequency, Hz |
| g | Acceleration of gravity, $m/s^2$ | θ | Wave direction |
| H | Wave height, m | ɸ | Latitude, degrees |
| h | Wave depth, m | φ | Velocity potential, $m^2$ /s |
| J | Energy flux, W/m | ρ | Density of sea water, $kg/m^3$ |
| k | Wave number, $(2\pi/\lambda)$, 1/m | λ | Wave length, m |
| m | Mass, kg | ω | Angular frequency, rad/s |
| M | Spectral moment, Nm | ζ | Vertical surface displacement, m |
| N | Wave action density spectrum, $m^2$/Hz | τ | Momentum of flux, $J/(m^2s)$ |
| | | ω | Angular frequency rad/s |

# 1. INTRODUCTION AND LITERATURE REVIEW

Ocean and sea waves carry very large amounts of energy that can be used to generate electricity, which contributes to reducing global warming rates and reducing the demand for electricity produced from oil [1]. Globally, the resource's estimated wave power is more than 2 terabytes [2]. Abidur et al. [3] mentioned that nowadays, the use of sea and ocean waves to generate electric power is very common and futuristic. Omar et al. [4] conclude that the energy of the sea and ocean waves is one of the most reliable, powerful, and attractive renewable energy sources, it is equivalent to (2-3 kWh/m²), wind energy (0.4 - 0.6 kW/m²), and solar energy (0.1-0.2 kWh/m²). Farrok et al. [5] state that wave energy has the most important renewable energy sources with many advantages compared to other types of renewable energies. In the northeastern region of Bari Island, the wave energy is 550 J/m2 [6]. However, the use of these energies requires long beaches, and this is what characterizes the Kingdom of Saudi Arabia, where wave energy is obtained from converting the periodic movement of waves up and down from placing equipment on the surface of the water, then these mechanical energies are captured and converted into electrical energy. The Kingdom of Saudi Arabia [5,6] is aware of the importance of renewable energy such as solar energy, wind energy, and sea wave energy,

and has huge oil resources. It is very interesting in taking an active role in developing new technologies to exploit and benefit from all kinds of renewable energies. Ralston et al. [7] concluded that waves are always high in most parts of the Red Sea and that the height of a large wave in its deep water ranges between 2.0 and 4.5 meters.

European countries have been at the forefront of ocean energy production [8], and in 2014, Bellamis produced around 250 MWh of electricity for the UK grid [9]. Ocean Energy Technologies [10] built a raft that converts wave energy into electricity at a rate of 1 kilowatt using an electric buoy and a piston that rises and falls with the movement of the waves and is connected to an electric generator. The average wave power along the Indian coast is about 5-10 kW/m and can produce 3750-7500 MW when only 10% of its energy is used [11]. The total available wave power globally [12] has been estimated at 2.7–70 TW, and in the Red Sea region, it is 5–10 kW/m. Despite all of the above, the performance of many wave energy companies was weak due to their inability to generate electricity from these high-energy waves due to the dependence of the devices that were used on the wave dynamics [13-17]. But currently, there are many different types of ocean wave energy converters (WECs) that have been successfully tested [18-20] to convert wave energy into electrical energy.

On the other hand, the wave conversion energy devices can be either rotational or transitional, and each type has different characteristics [21-23]. The

first type is linear generators (LGs), which convert wave energy directly without intermediate devices [24-26]. The second type is a transducer with thin floats, damping plate, and tensioned line system (which can provide good stability for better operating conditions) [27]. These devices are usually on or near beaches and produce power from 500 kW to 2 MW depending on the size of the systems. The third type [28] is to use the forces of reciprocating waves to transform the energy of the waves into a rotating movement in the floating vertical columns through rotating gears directly with the electric generators. The fourth type [29] is based on transforming the energy of reciprocating waves into pistons and air pressure in the tubes into wind turbines into electric generators. OPT has developed a system of easy-to-install wave buoys to produce 10,100 megawatts of electricity from the shores of Australia at a cost of about 3-7 cents/kWh. Wave energy works about 90% of the time while solar or wind generators only work 20-30% of the time and this makes the economic yield of wave energy suitable for wide power generation. A system of buoys with wave energy transducer (WEC) was installed with measurements taken for 12 months [30], and the results showed that the energy produced did not vary with wave climate. Despite the presence of the four previously listed, there is no data to compare between these types in terms of the best efficiency or the easiest to apply and the most capable of generating a greater amount of electrical energy, and therefore the work required in these topics is very large when applied with the highest efficiency systems. One of the objectives of this work is to determine the best location for the wave transducer on the shores of the Jazan region in the Red Sea. And deducing the most appropriate system for generating wave energy based on the information collected from satellite images and research published on this topic. Also, the effects of the wave depth, amplitude, length, and frequency are investigated. These parameters were evaluated along with environmental factors for sustainability development, site constraints, technical, and social impacts.

## 2. WAVE ENERGY RESOURCE ASSESSMENT FOR THE RED SEA

From the interesting properties of the seawater is the wave speed is proportional to its length ($C=gT/2p$). That is, longer waves will travel at higher speeds while the opposite is true for shorter waves. Wave energy is an intermittent energy source and Aboobacker et al. [31] concluded that the wave strength was calculated using the stopped wave parameters over 32 years, and the monthly, seasonal and annual wave strengths were estimated in the Red Sea. The results concluded that deep water gives the highest average wave power of 4.5 kWh/m² in the fall. In winter, the power of wave energy is given up to 6.5 kWh/m², in spring up to 5.0 kWh/m², and in summer up to 4.5 kWh/m². The highest mean wave energy is between seasons of Dec. to Mar, which is up to 6.5 kWh/m², the lowest during Jul-Aug (up to 4.0 kWh/m²). The bottom of the Red Sea is characterized by the power of waves laden with energy. The highest long-range average wave energy located along the central coast of Saudi Arabia is estimated at 1.6 kWh/m². Summer has the highest average wave power along the coast of Saudi Arabia with wave energy of 1.7 kWh/m² in the central region. In all seasons, the southern part of the coast of Saudi Arabia responds with low average wave energy (up to 0.41 kWh/m²). In the monthly rating, the average wave strength is higher along the western coast of Saudi Arabia approximately and constant during the period from January to September. And weaker during the period from October to November. And they estimated that the trends are positive across all sites with an average increase in mean wave strength of 20%, and under neutral conditions, the mean annual wave energy pattern is similar across all sites in the Red Sea, and this helps wave power converter (WEC) developers and operators in their decision.

It is not possible to predict the strength of waves and the time of their occurrence at a particular time, and this is the case for most renewable energy sources such as wind, waves, and the sun. Wind power is less intermittent than solar energy, and wind power at sea is less intermittent than wind power on land [32-34]. Wave energy is compared to wind energy, both because the two energy sources have a lot in common physically. The sea surface is lying on $xy$ plane, where $y$ component concerning zero as the wave

propagates in $x$-direction, $dW$ is the water depth of the sea concerning $xy$ plane or water surface, the seabed is at $z=-dW$, and the sea surface coincides with $z=0$. Then the general description of sea wave is depending on the interpretation of $\zeta=A\cos(kx-\omega t)$, where $\omega$ is the frequency, $[\omega=gk\tanh(kd_w)]^{0.5}$, that asserts the physics and describes consideration of a water wave relating frequency, $k$ is the number of waves ($k=2\pi/\lambda\omega$), $\upsilon$ is the phase speed or sea wave velocity. Figure 1 shows the waveform and amplitude of the free seawater wave. Hence, the perpendicular distance between the wave crest and trough is $H$ which is twice the amplitude $A$.

Considering the phase speed which is a single basic wave that moves along the $x$-direction can be expressed is:

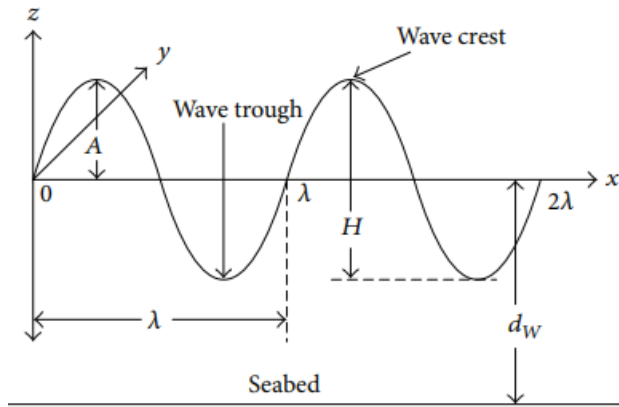$$\upsilon = [(gh/2\pi)\tanh(2\pi d_w/\lambda)]^{0.5} \tag{1}$$



**Fig.1.** Waveform and amplitude of free seawater wave

If the kinetic energy per unit length in x- direction is Ek, then the particle kinetic energy of width dx is:

$$dEkdx = 0.5dxdy\rho(r\omega)^2 = 0.5\rho\omega^2 a^2 e^{2y}dy = \rho\omega^2 a^2/4k \tag{2}$$

The total energy of the wave is:

$$dEk = 0.5\rho a^2 g = \rho a^2 g\lambda/4 = \rho a^2 T^2/4\pi \tag{3}$$

The power associated with the wave per unit width, (P/h=W/m) is:

$$P/h=(1/8\pi)\,\rho a^2 g^2 T \tag{4}$$

Based on the conservation of energy, since the source is the wave energy stream, the rate of change of the wave energy spectrum E(k) can be expressed [35] as:

$$\frac{dE(k)}{dt} = -[2k\sigma E(k)/(g\sinh^2 kd)]\int_{-d}^{0}\tau k\sin h(2kz + 2kd^2\,dz) \tag{5}$$

And in case of deep-water waves, Equ.5 becomes:

$$dE(k)/dt = -4k\sigma E(k)/g\int_{-d}^{0}\tau k\,e^{2kz}\,dz \tag{6}$$

Equation-6 shows the appropriate description of the waveform change based on the appropriate description of the turbulence changes on the wavelength scale, including the short-wave fraction modulation of the long-wave. The deep sea water dispersion relation can also be used to find a relationship between the wave length and the period of a wave. The phase speed which moves along the $x$-direction can be expressed as:

$$c_p =[(\lambda g/2\pi)\tanh(2\pi d_W/\lambda))]^{0.5} \tag{7}$$

According to Faraday's law, the induced voltage of the wave is:

$$E(t) = -Nd\Phi/dt \tag{8}$$

According to marine scientists, it is considered a linear wave, where the sea surface is lying on $xy$ plane, $y$ components are considered zero as the wave propagates in $x$-direction, $d_W$ is the water depth of the ocean concerning water surface ($xy$ plane), the seabed is at $z=-d_W$, and the ocean surface coincides with z=0. If the velocity potential is defined as, $\phi= (gh/2\omega)e^{kz}\sin(kx-\omega t)$, The flux variation concerning time can be expressed as:

$$\Phi(t) = 2\pi\Phi d_{tr}(t)/\lambda \tag{9}$$

The wave energy flux over the depth is described by pressure times velocity which can be written as integrate will give an expression for the flux per meter of wave crest:

$$J = -\int_{-\infty}^{0} pv_x\,dz \tag{10}$$

Combining Equs. (3-8 and 10), the average generated wave energy flux becomes:

$$J_m = 4\pi^2 A_w kN\Phi/\lambda T = \rho g^2 H^2 T/(32\pi) \tag{11}$$

Where p is the pressure, and if, the constant $\rho g^2/(32\pi)$ is denoted $\alpha$ in Equ. (11), using Equ. (7), the average generated wave energy flux can be written as:

$$J_m = \alpha k E c_p = \rho g^2 N\Phi/ (16\ \lambda)\ [(\lambda g/2\pi)\ tan(h)(2\pi l_W/\lambda)]^{0.5}(t) \quad (12)$$

However, the wave period (T) can be generated by using, T=3.55h0.5 (s), and the wave length ($\lambda$) can be generated by using $\lambda$ =5.12T2 (m), which equals 64.5248h (m). Figure 2 shows the effect of the sea waves period and height on the energy flux and production. It is noted from the figure that the energy produced by the waves increases with the increase in the height of the waves and decreases with the increase of the wave period. It should be mentioned here that the wave energy was calculated using the wave data and the number of occurrences of each wave condition according to the laboratory results of Rafael et al. [35]. The sea wave energy and power respectively can be written as the following:

$$E_w= 32.3\rho whga^2,\ E_{wd} = 0.5\rho ga^2 \quad (13)$$

And,

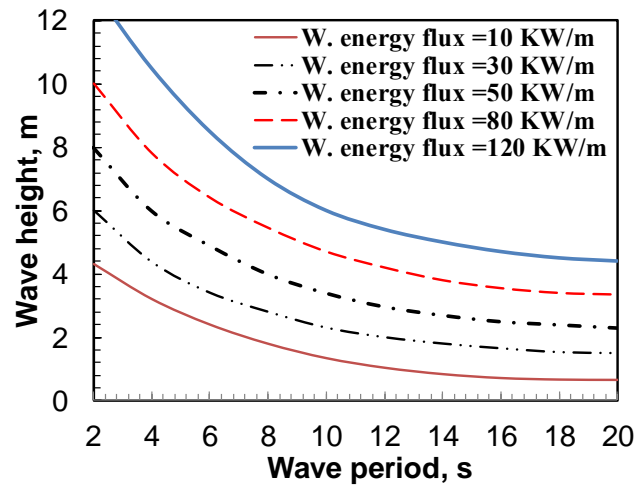$$P_w = 0.28h^2E_w\ ,\ P_{wd} = h^2E_{wd} \quad (14)$$



**Fig. 2.** Effect of sea wave period and height on the energy production

Where $E_w$ is the wave energy, w is the wave reflector length, $E_{wd}$ is the wave energy density that can be harvested per area of the wave, $P_w$ is the power that can be produced by sea waves, and $P_{wd}$ is the power density that can be harvested per area of the wave. In the conditions of the deep water with assuming, k=$\omega^2$/g, cg=g/2$\omega$, T=2$\pi$/$\omega$, the total sea wave power P, using Equ.14 is:

$$P =\rho g^2H^2T/(64\pi) \approx 0.55\ H^2T \quad (15)$$

The power concerning the height and period of the wave as well as the specific power of the wave per width can be calculated according to the standards of the transient water in watts per meter as follows:

$$P_w = (\rho gH^2/32)[1 + \tanh(kd)][\sqrt{\frac{g}{k}\tanh(kd)}][1 + 2kd/\sinh(2kd)] \quad (16)$$

Using Equ. 16, for a given wave period and height, the wave power per meter can be evaluated of the crest of that wave as shown in figure 3. It is clear from the results that the power produced from sea waves is not constant, but it has maximum values of about 1.5 kW/m and minimum values ***close to zero, and the estimated average power of about 0.43 kW/m. This fluctuation in the wave power is due to the intensity of wind speed. In general, the power generated is greater than that of more powerful waves, which is determined by knowing the length and velocity of the wave and from the density of the water. Mathematically, wave power is determined by wave power equations whose factors are wave energy or wave energy flow and wave energy transfer rate. In general, in deep water, the two scientists consider the depth of water to be greater than half the wavelength. Robertson et al., [37] have been estimated the global wave energy of 2.11 ± 0.05TW. Figure 3 shows the power generated by the waves result of the current model. The average power of the sea waves is about 24% of the first load configurations of the buoy.
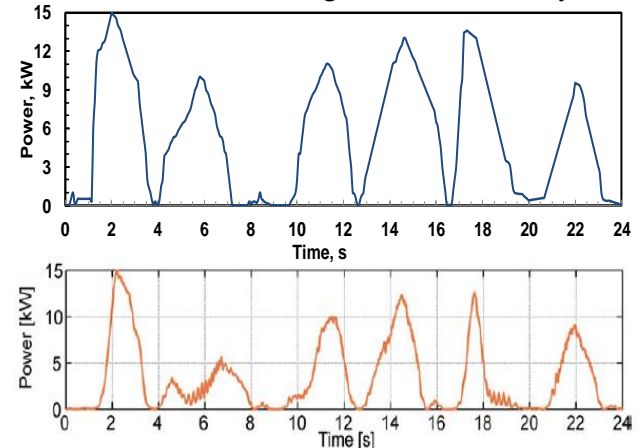
## 3. NUMERICAL WAVE MODELING

At present, numerical models are one of the most powerful tools for studying seawater waves and dams and predicting their energy. Also, they have proven to be an essential tool for the design and protection of coastal structures and as a life-saving tool during hurricanes and storms [38]. On the other hand, due to the irregular behavior of the sea waves, which have varying intensities, the intensity of the contrast E(f) can be written instead of Equs.8 and 10 as E(f)=0.5a(f)²Δf. And the energy of the omnidirectional wave (J) that can be transferred as the energy passes through a cylinder of a hypothetical unit diameter can be written as:

$$J = \rho g \sum_i c_{g,i} E_i \Delta f_i \qquad (17)$$

Where, $c_{gi}$ is the wave group velocity, ($c_{gi}=(\pi f_i/k_i)[1+2k_ih/(\sinh(2k_ih)])$), $f_i$ represents the $i^{th}$ wave frequency in the spectrum, $\Delta f_i$ is the frequency bandwidth, $k_i$ is the wave number ($2\pi/L$) and $h$ is the water depth. Most of the factors that are used to describe the spectra of waves depend on the spectral moment ($M_n$), which be written as:

$$M_n = \sum_i f_i^n E_i \Delta f \qquad (18)$$

And if the height of the zero-momentum wave ($H_{mo}=4\sqrt{M_n}$), is considered, the total energy of sea waves from all directions at the same time (directed wave energy, $J_\theta$) is:

$$J_\theta = \rho g \sum_{i,j} c_{g,i} s_{i,j} \Delta f_i \Delta \theta_j (\theta - \theta_j)\delta \begin{cases} \delta = 1, \cos(\theta - \theta_j) \geq 0 \\ \delta = 0, \cos(\theta - \theta_j) < 0 \end{cases} \qquad (19)$$

Equation 19 indicated that the weighting of the cosine function and Jθ take priority for wave systems whose directions have the height energy transfer and minimize the effect of low wave energy flow from transverse directions. Provide the coefficient d (=JqJmax/J) the directional of spreading wave in the directional of the space, and $\epsilon_0$ the measure of the spreading wave across the frequency space. Langodan et al. [39] mentioned that all large mathematical models underestimate the energy produced from sea and ocean waves, which led to a

lack of great interest to produce electricity from them, and this is what laboratory experiments have proven the opposite. When the wave conditions are known within 20 minutes, the wave power can be evaluated using Equ.15, and substitute, P = 0.55H2sTz, kW/m, the average height of the wave Hm, and the height of the big wave Hs (average top 33% of waves). Figure 4 introduces a comparison between the results of the current model and practical measured by NDBC buoys of [29], and what they stated is confirmed in this figure. It is noted in this figure that the spectra of high-frequency energy waves are few, despite the high value of energy production from these waves, which proved that the cost of kilowatt-hours is lower than that of wind, solar, and hydraulic energies as mentioned in the reports of researchers in this field [4, 5, 11, 12].
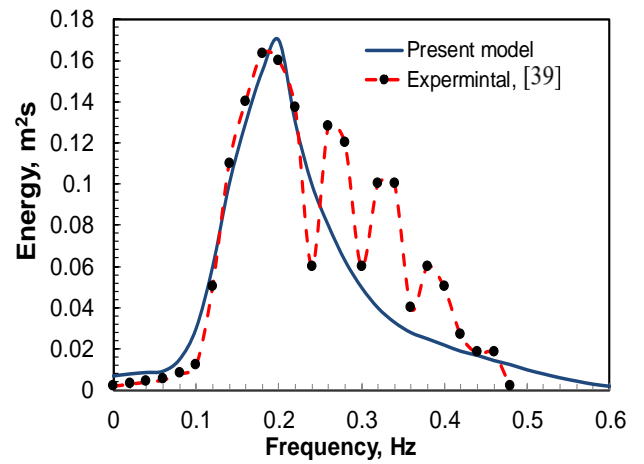


**Fig. 4.** Comparison between results of the present model and measured [39]

## 4. ESTIMATION OF POWER ASSOCIATED WITH WAVES

The intensity of the Doppler spectrum can be written based on the spectral theory of Doppler in the case of wave height within the cross-section as follows:

$$I(\omega) = (2\sigma\pi^{2.5}V_ST_S/h^2)exp[-(2/bt)^2\omega^2]\times exp[-(2/bt)^2(\omega-\omega_u)^2] \qquad (20)$$

And the generated voltage can be written as:

$$V_g(t) = V_m \cos(2\pi t/T) \cos\{(2\pi A_w/\lambda)\sin(2\pi t/T)\} \qquad (21)$$

Using Equs. (20, 21) the sea wave generated power as a function of time and period can be evaluated. Figure 5 shows the effect of wave period on the wave

energy absorption efficiency of buoys system at buoy boom length of 8.0 m, a radius of 1.0 m, and damping coefficient of hydraulic system 5.0 × 104 N/sec/m. It is clear from the figure that the absorption power of the device and the power of the incoming wave are varying with the period of the wave, and that the power of the incoming wave increases with the increase of the period of the wave. The absorbing capacity of the wave energy from buoys and the hydraulic system is maximum when the wave period is 3.7 seconds and 3.2 seconds respectively and then starts to decline. Figure 5 shows the Red Sea mean wave period through a year from the results of the present model. The figure shows the different values of the wave period during the various months due to the changes in the speeds and strengths of sea waves resulting from the variations in the wind speed that is completely associated with it. The figure shows that the average in some months differs from other months, i.e., the wave period January is weak, but in July it is strong. Every month, a change in the wave force is observed from one day to another day, and the results of the current theoretical model and laboratory results of Aboobacker et al. [31] are in agreement despite some minor differences in the severity of the mortality for some days. The average mean wave period in the present model is at about 4.3s while the experimental at 4.6s. The maximum values of the mean wave period are about 8s and the minimum is about 2 in the experimental and model.
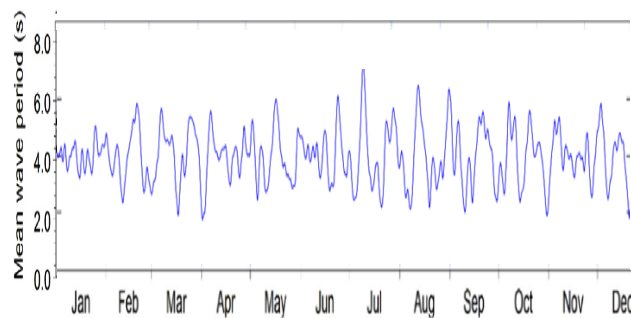


**Fig. 5.** Comparison between the results of the present model

Figure 6 shows the effect of wave height on the power generated from the sea wave of the present model and experimental data of Rafael [35]. The figure show increases in wave-generated power period energy produced by waves at different heights of these

waves. The figure shows when the waves height increase, the resulting power increases steadily. The laboratory results of Rafael [35] and the current theoretical model give an approximation to the results. Rafael et al. [41] found that the average power flux is about 5.2 kW/m at offshore Skagerrak of Sweden, 2.8 kW/m near Skagerrak beach, and 2.4 kW/m at Kattegat. While the average power flux above 55 kW/m (ten times the general average) only during 7 days of the 8 years studied and exceeds 100-250 kW/m only during half an hour (the highest 45 times the overall average). But the power flow reaches above 13.5 kW/m only 10% of the time. Almost 50% of the total energy is found in offshore nations with a large wave height between 1 and 3 meters and a power period between 4 and 7 seconds.
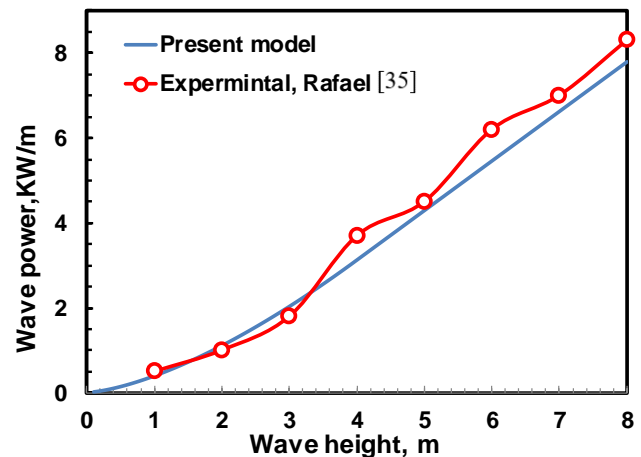


**Fig.6.** Effect of wave height on the sea wave power from the present model and Exp. [35]

## 5.     ESTIMATION OF THE RED SEA WAVE ENERGY IN THE JIZAN REGION

Data were collected from satellite images and previously published research [12, 33, 35, 39 - 41] on the power of the Red Sea waves. Also, from the collected data of satellite images, the values that published by the researcher Aboobacker et al. [23], and using the above-mentioned equations in the current work, the sea wave produced energies in the Jazan area in the period from 2012 to 2021 is assessed, and represented in the Fig. 7 for the different locations and Fig. 8 for different months of a year. Some locations of those are selected at Jizan city from the north to south of the red sea as the following: Al Shuqaiq beach B1, Bayesh beach B2, Al Tarfa beach B3, Al Hizam beach B4, Al Murjan

Beach B5, Al Madaya beach B6, Al Mawasem beach Y7, Farasan Island beach B8, Muharraq beach B9, Janaba beach B10, Al Khattab beach B 11, Saber beach B12. The data of sea wave energy in the specified places from B1 to 12 for the beaches of Jizan city for the different seasons were represented in Figure 8, which shows that the intensity of wave energy on Al Shuqaiq beach L2 is the highest for the study areas followed by Al Murjan Beach B5, then Al Madaya 6. Figure 8 shows the highest wave energy at the location Al Shuqaiq beach B1. It is clear from Fig.8 that the highest sea wave energy is in January and December and decreases during the summer season.
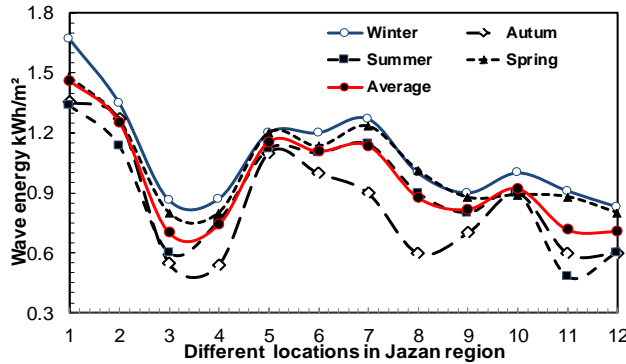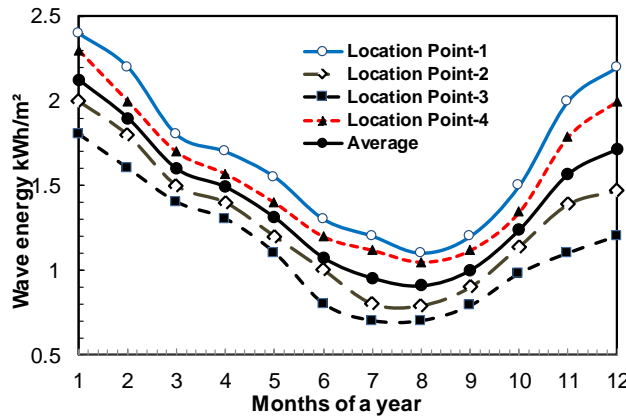


**Fig. 7.** Sea wave energy at a different location



**Fig. 8.** Wave energy through a year for different four locations

## 6. VARIATION OF WAVE ENERGY ABSORPTION EFFICIENCY WITH THE RADIUS OF THE BUOY

Since the sea wave energy depends entirely on wind energy, which is very large in the Kingdom of Saudi

Arabia, so many researchers confirmed that wave energy is promising economically in this country [42-44)]. The effect of the diameter and tensioned conduction line of the buoy which is used to generate electricity from sea waves on its performance was studied [45-49]. And because the speed of a wave is proportional to its length so the longer waves will travel at higher speeds and vice versa for shorter waves. Wang et al. [51] reported that the buoy has an efficiency of 98% of wave energy when it has a radius of 1.8 m and produces slight harmonic vibrations affected by forces in the vertical direction. To study the power output from a floating transformer system consisting of a cylindrical transformer and a hydraulic transformer partially immersed in seawater. The force can be written according to Newton's second law respectively as [52]:

$$(m+m_w)\ddot{y} = F_C + F_S + F_V \tag{22}$$

Where m is the mass of the buoy, $m_w$ is the mass added of the buoy ($m_w = \pi \rho R^2/2$), $F_C$ is the equivalent damping force $\{F_C = [(-8CR^2/L^2)(1-r)\dot{y}]\}$, $F_S$ is the hydrostatic restoring force ($F_S = \rho g Y A_{WP}$), $F_V$ is the wave force ($F_V = F_0 \cos \omega t$), $F_0$ is the amplitude of wave force that can be solved by the methods of theoretical analysis or, $\omega$ is wave circular frequency, $\ddot{y}$ is the heaving motion accelerated speed, $A_{WP}$ is the buoy wetted surface ($A_{WP} = 2L(2dR-d^2)^{0.5}$), d is the buoys immersed depth, L, R, are the buoy cylinder length and radius respectively, C is the damping coefficient, ($C = v_c/f$), f is the hydraulic damping force, $v_c$ is the speed of hydraulic cylinder piston, r is introduced as the proportionality coefficient of speed ($r = \dot{y}_o/\dot{y}$), y is the displacement of buoys heaving motion, and $\dot{y}$ the speed. Using the above definition of the different forces with Equ.22, the equations of motion of buoys can be written as:

$$F_0 \cos \omega t = (m+m_w)\ddot{y} + (-8C R^2/L^2)(1-r)\ddot{y} + rgZA_{WP} \tag{23}$$

the buoy wave energy absorption power, $P_c$ can be written as:

$$P_C = (C/T)\frac{C}{T}\int_0^T [2(1-r)Ry)/L]^2 \, dy \tag{24}$$

and the wave energy absorption power of buoys is:

$$P_F = \frac{1}{T}\int_0^T F_V \, y dt \tag{25}$$

It is possible to estimate the variation in the absorption power and the incoming wave power with

the wave period with the buoy and hydraulic systems using Equs. 22-23. The results of the present solution at the condition of buoy length of 8.0m, the radius is 1.0m, and the damping coefficient of the hydraulic system is $5.0 \times 104$ N·s/m at different wave periods are shown in figure 9. The effects of the wave period on the wave incoming power, buoys, and hydraulic system are shown in the figure. The figure shows that the wave energy absorption power of the floats is maximum when the wave period is 3.6 seconds and 3.2 seconds respectively and then starts to decline. Therefore, the power of the incoming wave is a secondary factor that affects the dynamic responses of wave-capturing floats at a fixed wave height. Figure 10 shows the effect of buoys length on the average generated output powers according to the model. So we can get the conclusion that the model that we established in this paper is effective and available. The figure shows the buoys and the hydraulic system energy absorption power of the wave reaches its maximum at a submerged depth of about 1.5 m begins to drop sharply and reaches less than 10% at a submerged depth exceeding 1.8 m. It can explain that because the growth rate of the wave force exceeds the growth rate of the mass inertia in the initial stages, the area of the immersed float decreases rapidly that leading to a decrease in the wave force. It means the efficiency drops more quickly due to the combined action of lower wave power and greater mass inertia. The power output from the wave increases with the increase of the wave height and buoy length as well as radius. The sea wave energy conversion efficiency can be expressed as the wave energy absorption efficiency similar to Ruellan et al. [53] and using Equs. 22 - 25 as:

$$\eta_f = P_F/P_{Sea}, \; and \; \eta_c = P_C/P_{Sea} \qquad (26)$$

Where, $\eta_F$ and $\eta_C$ are the wave energy absorption efficiency of buoys and hydraulic system respectively, $P_F$, and $P_C$ are the average wave energy absorption power of buoys and hydraulic system, $P_{Sea}$ is the input power of the wave, ($P_{Sea} = \rho g^2 BTH^2/32$) [54], B is the immersed width of buoys. Figure 11 shows the effect of buoy radius on the efficiency of the wave energy absorption efficiency. It is in the figure that both wave energy absorption efficiency of buoys and hydraulic systems attain their maximum when its radius is about 1.8 m. The maximum efficiency of the wave energy absorption of the buoys and hydraulic systems is 98% and 80% respectively.
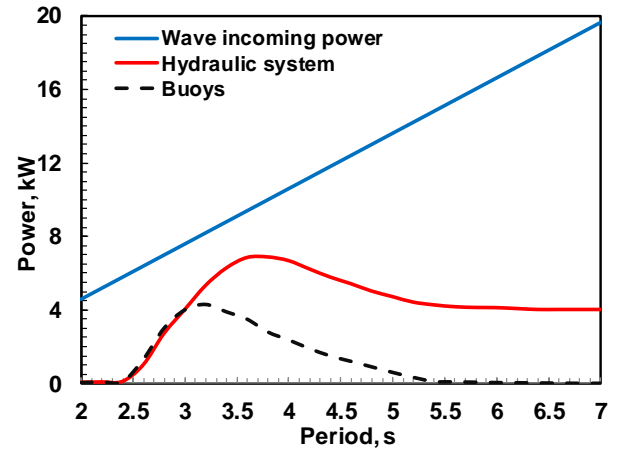


**Fig.9.** Variation of absorbing power of device and incoming wave power with wave period
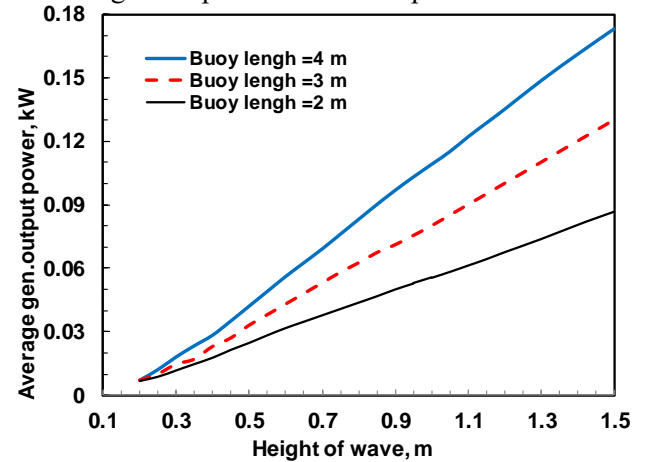


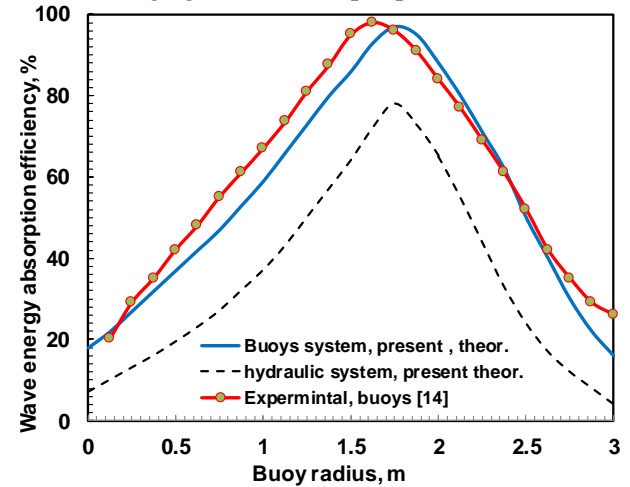**Fig.10**. Effect of buoy length and wave height on wave average generation output power



**Fig. 11**. Effect of buoy radius on the wave energy absorption efficiency

## 7. CONCLUSIONS

This research studies the use of the waves energy of the Red Sea shores of Jazan city to generate electric power using the system of buoys. The buoy motion was derivative according to the wave parameters factors of Newton's second law and on the linear wave theory. The weather assessment of the wave off the western coast of Jizan, Saudi Arabia was assessed based on the compilation of data from satellite imagery and published research for 10 years for 12 sites. Several twelve places along the coasts of Jizan city using satellite images and published research was surveyed to find the most suitable places for the highest wave energy. Effect of buoy system design parameters that effects the efficiency of absorbing wave energy were discussed. It was found that the buoy design factors such as the length, radius of the buoy, and the submerged depth of the buoy are of great importance for the absorption of the wave energy.

It was found that the beach of Al Shuqaiq area is the best place from the beaches of Jizan city to install the buoy and obtain the highest electric energy due to the presence of the highest wave intensity, followed by the beach of the Baysh and Al Marjan area. The highest marine energy endurance case with an average power flux of 1.0 kW/m was found at Al Shuqaiq Beach. Wave heights are annually found in the interval 1-3 m and energy intervals in the period of 4-7 s. The wave energy absorption power of the floats is maximum when the wave period is 3.6 seconds and 3.2 seconds. The results showed that the main factor affecting the dynamic responses of wave-capture buoys is the proximity of the natural frequency of buoys to the wave period. The length and radius of the buoy are the most important factors influencing the design of the buoys to increase the energy of the waves, along with the submerged depth of the buoy. The present theoretical results were compared with the laboratory results of the published research and showed agreement to an acceptable degree.

## 8. REFERENCES

[1] Vivekraj, M., "*Design and Development of Ocean Wave Energy Power Generation System*", Int. J. of Eng. Res.& Tech. (IJERT), Published by: www.ijert.org Vol. 10, Issue 03, March 2021. 91-92

[2] Gunn, Kester, and Clym Stock-Williams. "Quantifying the global wave power resource." *Renewable Energy* 44 (2012): 296-304..

[3] Rahman, Abidur, et al. "Recent progress in electrical generators for oceanic wave energy conversion." *IEEE Access* 8 (2020): 138595-138615.

[4] Farrok, Omar, et al. "Electrical power generation from the oceanic wave for sustainable advancement in renewable energy technologies." *Sustainability* 12.6 (2020): 2178.

[5] Farrok, O., Islam, M., and Sheikh, M., "Analysis of the Oceanic Wave Dynamics for Generation of Electrical Energy Using a Linear Generator," J. of Energy 2016 (2016): 1-14.

[6] Vidura A., Nurjaya W., Iqbal M., Jaya I "Ocean wave measurement and wave energy calculation using overtopping power plant scheme." *IOP Conference Series: Earth and Environmental Science*. Vol. 429. No. 1. IOP Publishing, 2020..

[7] Ralston, David K., Houshuo Jiang, and J. Thomas Farrar. "Waves in the Red Sea: Response to monsoonal and mountain gap winds." *Continental Shelf Research* 65 (2013): 1-13.

[8] Misaa A., Tayeb B., and Sabique L., Alkhayyat, "Wave energy converters: Barriers and drivers." (2020).

[9] Neill, Simon P. "Introduction to Ocean Renewable Energy." *Reference Module in Earth Systems and Environmental Sciences, Elsevier* (2021).

[10] Al Yousif, Mohammed Ahmed, and Al Yousif. "Renewable Energy Challenges and Opportunities in the Kingdom of Saudi Arabia." *International Journal of Economics and Finance* 12.9 (2020): 1.

[11] Esteban, Miguel, Alexandros Gasparatos, and Christopher NH Doll. "Recent developments in ocean energy and offshore wind: financial challenges and environmental misconceptions." *Sustainability through innovation in product life cycle design* (2017): 735-746..

[12]    Mork, Gunnar, et al. "Assessing the global wave energy potential." *International Conference on Offshore Mechanics and Arctic Engineering*. Vol. 49118. 2010.

[13]    Amir, Mohamad Abu Ubaidah, et al. "Wave energy convertors (WEC): A review of the technology and power generation." *AIP Conference Proceedings*. Vol. 1775. No. 1. AIP Publishing LLC, 2016.

[14]    Gao, Hongtao, and Biao Li. "Establishment of motion model for wave capture buoy and research on hydrodynamic performance of floating-type wave energy converter." *Polish Maritime Research* 22.S1 (86) (2015): 106-111.

[15]    Staneva, Joanna, et al. "Effects of wave-induced forcing on a circulation model of the North Sea." *Ocean Dynamics* 67.1 (2017): 81-101.

[16]    Alawaji, Saleh H. "Wind energy resource assessment in Saudi Arabia—I. Network design and description." *Renewable Energy* 7.4 (1996): 319-328..

[17]    Rehman, Shafiqur, T. O. Halawani, and M. Mohandes. "Wind power cost assessment at twenty locations in the Kingdom of Saudi Arabia." *Renewable Energy* 28.4 (2003): 573-583.

[18]    Ralston, David K., Houshuo Jiang, and J. Thomas Farrar. "Waves in the Red Sea: Response to monsoonal and mountain gap winds." *Continental Shelf Research* 65 (2013): 1-13..

[19]    Thorburn, Karin. *Electric energy conversion systems: wave energy and hydropower*. Diss. Acta Universitatis Upsaliensis, 2006.

[20]    Drew, B., Plummer, R., and Sahinkaya, N., "A Review of Wave Energy Converter Technology", J. of power energy, Proc. IMechE, Vol. 223, Part A, pp. 887-902, 2009.

[21]    Tolman L., Balasubramaniyan B., Burroughs D., Chalikov V., Chao Y., Chen S., and Gerald M., Tolman "Development and implementation of wind-generated ocean surface wave modelsat NCEP." *Weather and forecasting* 17.2 (2002): 311-333.

[22]    Rehman, Shafiqur, and Aftab Ahmad. "Assessment of wind energy potential for coastal locations of the Kingdom of Saudi Arabia." *Energy* 29.8 (2004): 1105-1115.

[23]    Komen J., Cavaleri L., Donelan M., Hasselmann K., Hasselmann S., and. Janssen M, "Dynamics and Modelling of Ocean Waves",

Cambridge University Press, Cambridge, 532 pp, 1994.

[24]    Sherif, Ahmed Moheb, H. E. El-Mors, and Z. E. Ismail. "Generating The Electrical Energy from Sea Waves." *Journal of Soil Sciences and Agricultural Engineering* 10.12 (2019): 805-813.

[25]    Soerensen, H. C., and S. Naef. "Report on technical specification of reference technologies (wave and tidal power plant)." *NEEDS Project Rep* (2008).

[26]    Witt, M. J., et al. "Assessing wave energy effects on biodiversity: the Wave Hub experience." *Philosophical Transactions of the Royal Society A: Mathematical, Physical and Engineering Sciences* 370.1959 (2012): 502-529.

[27]    Arshit A., Jay D., Mehul K., Shahnawaz A., and Zaid A., "Generation of Electricity from Ocean Waves", Int. Res. J. of Eng. and Tech. (IRJET) 03 (04) (2016): 1-14

[28]    Al-Abbadi, Naif M. "Wind energy resource assessment for five locations in Saudi Arabia." *Renewable Energy* 30.10 (2005): 1489-1499.

[29]    Şahin, Ahmet Z., and Ahmet Aksakal. "Wind power energy potential at the northeastern region of Saudi Arabia." *Renewable Energy* 14.1-4 (1998): 435-440.

[30]    Rehman, Shafiqur, and Naif Al-Abbadi. "Wind power characteristics on the North West coast of Saudi Arabia." *Energy & environment* 21.8 (2009): 1257.

[31]    Aboobacker, V. M., et al. "Wave energy resource assessment for Red Sea." *Renewable Energy* 114 (2017): 46-58.

[32]    Huang, Lei, et al. "Winding configuration and performance investigations of a tubular superconducting flux-switching linear generator." *IEEE Transactions on Applied Superconductivity* 25.3 (2014): 1-5.

[33]    Zhen, L., Cui Y., Zhao H., Shi H., and Hyun S. "Effects of damping plate and taut line system on mooring stability of small wave energy converter." *Mathematical Problems in Engineering* 2015 (2015).

[34]    Tolman, H. L. "the WAVEWATCH III Development Group: User manual and system documentation of WAVEWATCH III version 4.18." *Technical Note, Environmental Modeling Center, National Centers for Environmental Prediction, National Weather Service, National*

*Oceanic and Atmospheric Administration, US Department of Commerce, College Park, MD* (2014).

[35] Waters, Rafael. *Energy from ocean waves: full scale experimental verification of a wave energy converter*. Diss. Universitetsbiblioteket, 2008.

[36] Kamranzad, B., A. Etemad-Shahidi, and V. Chegini. "Assessment of wave energy variation in the Persian Gulf." *Ocean Engineering* 70 (2013): 72-80.

[37] Robertson, B., "Wave Energy: Resources and Technologies", Reference Module in Earth Systems and Environmental Sciences, 2021.

[38] Thomas, T. Justin, and G. S. Dwarakish. "Numerical wave modelling–A review." *Aquatic procedia* 4 (2015): 443-448.

[39] Langodan, Sabique, et al. "The Red Sea: a natural laboratory for wind and wave modeling." *Journal of Physical Oceanography* 44.12 (2014): 3139-3159.

[40] Chenari, Behrang, Seyedeh Shiva Saadatian, and Almerindo Ferreira. "Wave energy systems: An overview of different wave energy converters and recommendation for future improvements." *Proceedings of the 8th International Technology, Education Development Conference, Valencia, Spain*. 2014.

[41] Waters, Rafael, et al. "Wave climate off the Swedish west coast." *Renewable energy* 34.6 (2009): 1600-1606.

[42] Bidlot, Jean-Raymond, et al. "A revised formulation of ocean wave dissipation and its model impact." (2007): 27.

[43] Mendes, Lourenço, et al. "Analysis of the impact of a pilot zone for wave energy conversion offshore Portugal." *The Eighteenth International offshore and polar engineering conference*. OnePetro, 2008.

[44] Setoguchi, T., et al. "Air-turbine with self-pitch-controlled blades for wave energy conversion (estimation of performances in periodically oscillating flow)." *International Journal of rotating machinery* 3.4 (1997): 233-238.

[45] Said, S. A. M., I. M. El-Amin, and A. M. Al-Shehri. "Renewable energy potentials in Saudi Arabia." *Beirut regional Collaboration Workshop on energy efficiency and renewable energy technology, American University of Beirut*. 2004.

[46] Rehman, Shafiqur, and Naif M. Al-Abbadi. "Wind shear coefficient, turbulence intensity and wind power potential assessment for Dhulom, Saudi Arabia." *Renewable Energy* 33.12 (2008): 2653-2660.

[47] Rehman, Shafiqur, et al. "Wind power resource assessment for Rafha, Saudi Arabia." *Renewable and Sustainable Energy Reviews* 11.5 (2007): 937-950.

[48] Elhadidy, M. A., and S. M. Shaahid. "Wind resource assessment of eastern coastal region of Saudi Arabia." *Desalination* 209.1-3 (2007): 199-208.

[49] El-Tamaly, H. H., M. Hamada, and Ali M. EL-Tamaly. "Computer simulation of wind energy system and applications." *Proceedings international AMSE conference in system analysis, control & design*. Vol. 4. 1995.

[50] Sun, Z. F. "Research of oscillating buoy wave energy device." *Shanghai: Shanghai University* (2007): 31..

[51] Wang, X. N., X. L. Li, and J. Wang. "Study on the assessment of performance of the wave energy conversion systems." *Ocean Technology* 31.4 (2012): 75-78.

[52] Gao, H. T., S. F. Guan, and D. L. Zhou. "Experimental test on a kind of floating-type wave energy converter." *Acta Energiae Solaris Sinica* 34.1 (2013): 177-180.

[53] Ruellan, Marie, et al. "Design methodology for a SEAREV wave energy converter." *IEEE Transactions on Energy Conversion* 25.3 (2010): 760-767.